



Geomorphic and paleoseismological evidence of active Kachchh Mainland Fault, Kachchh, India

Girish Ch Kothyari¹ · Raj Sunil Kandregula¹ · Gaurav Chauhan² · M. G Thakkar²

Received: 12 March 2018 / Accepted: 25 April 2020 / Published online: 13 June 2020
© Saudi Society for Geosciences 2020

Abstract

The present work pertains to the stratigraphic evidences found during paleoseismic investigations on the trench walls opened across the Kachchh Mainland Fault (KMF). High-resolution satellite (CARTOSAT-1 DEM) data is used for mapping fault traces and carried out paleoseismic studies to identify paleo-earthquakes. We undertook geomorphological and paleoseismological investigations along the central segment of the KMF zone with the aim of estimating long-term slip rate and recurrence interval of strong earthquakes. Two N-S trenches were excavated across the E-W striking branches of the KMF, named as KMF-1 and KMF-2, revealing that the KMF is dipping towards the north. Detailed studies of the trench walls and optical dating of event horizons have confirmed four earthquakes occurred in the KMF zone between 5600 and 1000 years. The earthquake event I occurred between 5000 and 5500 years; event II occurred between 4000 and 4600 years. The event III occurred between 2000 and 2900 years, and the event IV occurred between 1023 and 1259 AD and 02 BC to 427 AD. Our studies further indicate that the central KMF zone is probably undergoing a quiescent period of ~ 1000 years accumulating the stress in the system to generate a large earthquake. The uplifted and truncated fluvial strath terrace deposits resulting from the Holocene displacements are preserved along the hanging wall block of the KMF. Dividing the elevation of the bedrock strath by their ages yields estimates of the vertical uplift rate of 0.37 to 1.48 mm/year of the hanging wall block of central KMF. With the help of displaced sedimentary units and optical ages, we estimated an average slip rate of 0.28 mm/year and uplift rate of 0.13 mm/year along KMF-1 over an interval of 1800–4000 years. However, the estimated slip rate along KMF-2 is 0.30 mm/year and the observed uplift rate is 0.17 mm/year. The results obtained from the trench investigations along the KMF not only help in understanding the dynamics of KMF but also aid seismic hazard evaluation in the Western Peninsular India.

Keywords Active fault · Paleoseismology · Earthquakes · Kachchh Mainland Fault

Introduction

The frequent occurrence of the large intraplate earthquakes causes a significant threat to population and infrastructure (Michetti et al. 2005; Massotti 2007). Such earthquakes may have occurred because of the weakening of lithosphere caused by a reduction of crustal and upper mantle strength owing to

thermal, mechanical, or chemical anomalies (e.g., Liu and Zoback 1997; Talwani and Acree 1984; Costain et al. 1987; Michetti et al. 2005). Quantification of the historic earthquake records, preserved in the recent Holocene surfaces (geological and geomorphic), is therefore called paleoseismology (Michetti et al. 2005). The earthquake records preserved in Holocene surfaces provides rates and impact of ongoing tectonics activity (in local and regional scale) and kinematic behavior of fault (e.g., Vittori et al. 1991; McCalpin 1996; Michetti and Hancock 1997; Yeats et al. 1997; Wallace 1984; Audemard 1999; Serva et al. 2002; Wesnousky 1988; Cowie 1998; Gupta et al. 1998; Wesnousky 2000; Roberts and Michetti 2004). Globally in an intraplate setting, the large earthquake occurs in areas, where lower lithospheric strength significantly reduced by thermal heat and an abnormal increase of higher stress concentration (Massotti 2007). For example, in the intraplate region of Canada, the earthquake

Responsible Editor: Mustapha Meghraoui

✉ Girish Ch Kothyari
kothyarigirish_k@rediffmail.com

¹ Institute of Seismological Research, Raisan, Gandhinagar, Gujarat 382007, India

² Department of Earth and Environmental Science, KSKV Kachchh University, Bhuj, India

occurred along Late Proterozoic–Cambrian Iapetan rift margin (Adams et al. 1995; Adams and Halchuk 2003; Massotti 2007). Similarly, the frequent earthquakes in the New Madrid seismic zone are considered to be induced by the amalgamation of a warmer geotherm, dense rift pillow, and the transient perturbation of Holocene postglacial rebound (Pollitz et al. 2001; Massotti 2007).

The intraplate Kachchh Rift Basin (KRB) of Western India is located southeast of seismically most active plate boundaries along Chaman Fault system and Makran Subduction zone (Malik et al. 2017). The KRB in the western margin of India evolved in successive stages during the migration of the Indian plate after its breakup from Gondwana during the Late Triassic along the major Precambrian trend (Biswas 1977, 1982, 1987). The Gondwana drifted away with a speed of 3–5 cm/year during the Middle Jurassic; because of the counterclockwise rotation, the Kachchh rift widened and a basin formed (Biswas 1982), which was filled with ~ 3000 m thick Mesozoic and Cenozoic sediments (Biswas 1987). During the Middle Cretaceous, Madagascar began rifting from Western India along the NNW-SSE trending Dharwar basement (Gombos et al. 1995). Around 66 Ma, the Deccan/Reunion hot spot erupted (Courtillet et al. 1986) and the western margin of India crossed the equator and passed over the hot spot (Biswas 1982). Extensive subaerial eruptions of several flows of flood basalts covered an area of about two million square kilometers now known as Deccan Traps (Biswas 1982; Talwani and Gangopadhyay 2001). The Indian landmass collided with Eurasia around Late Paleocene–Eocene time with a spreading motion of 4 to 6 cm/year (Dewey et al. 1989; Patriat and Achache 1984; Besse et al. 1984; Jaeger et al. 1989; Larson et al. 1999; Beck et al. 1995; Biswas 1982; Zheng et al. 2017). Thus, by the Late Miocene, the east-west trending KRB had formed and was being subjected to a north-south compressive stress field representing the structural response to stress reorientation associated with the Himalayan orogeny (Talwani and Gangopadhyay 2001). During the final stage, the maximum horizontal stress that is responsible for current tectonic activity is oriented N-S to NNE-SSW (Gowd et al. 1992; Biswas and Khattri 2002; Biswas 1977, 1987; Rastogi et al. 2014; Kothiyari et al. 2016c). The E-W oriented KRB was formed in the Late Miocene and is bounded by two major basin-forming faults, the south-dipping Nagar Parkar Fault (NPF) to the north and north-dipping Kathiawar Fault (KF) to the south (Biswas 1993; Fig. 1a).

The KRB experienced several moderate to large earthquakes during the historic past, such as the 2200 BC Dholavira earthquake (Mw 6.5; Bisht 2011), the Indus Delta earthquake that occurred between 712 and 1361 AD (Frere 1870; Williams 1958; Siveright 1907; Bilham 1998; Rajendran et al. 2008), the 1819 Allah Bund earthquake (Mw 7.8), the 1956 Anjar earthquake (Mw 6.0), and the 2001 Bhuj earthquake (Mw 7.7) (Oldham 1926; Bilham

1998; Chung and Gao 1995; Yagi and Kikuchi 2001; Johnston 1996; Rajendran and Rajendran 2001; Rajendran et al. 2001 and 2008; Bodin et al. 2004; Khan et al. 2016) (Fig. 1a). Among the recent events, the 1956 event originated at a shallower depth of < 10 km while the 2001 Bhuj event occurred at a greater depth (25 km). The 2001 Bhuj earthquake is the most destructive event to hit the intraplate region of Western Peninsular India (Talwani and Gangopadhyay 2001; Bodin et al. 2004; Khan et al. 2016). Out of these earthquakes, only the 1819 Allah Bund earthquake has been reported to had coseismic surface rupture, resulting in the formation of a fault scarp about 5–6 m high (Quittmeyer and Jacob 1979; Johnston and Kanter 1990). Further, during the 1819 Allah Bund earthquake (Mw 7.8), approximately 3–6 m uplift of landmass has been reported within the Western Great Rann (Oldham 1926, 1883; Burnes 1835; Baker 1846; Quittmeyer and Jacob 1979; Johnston and Kanter 1990; Bilham 1998; Rajendran and Rajendran 2001). Previous studies reveal that the 2001 Bhuj event occurred along a blind fault with no evidence of surface faulting (Mandal et al. 2004; Rastogi et al. 2014). However, evidence of surface rupture associated with the 2001 Bhuj earthquake has been reported by McCalpin and Thakkar (2003) and Kothiyari et al. (2015). The paleoseismic studies from the Great Rann of Kachchh (GRK) revealed evidence of large magnitude earthquakes those occurred during a time span of BCE 800–1000 (Rajendran and Rajendran 2001; Rajendran et al. 2008). Similarly, the archeological records from the central part of Mainland Kachchh suggest that the area was hit by an earthquake around 2200 BC (~ 3.5 ka) (Kothiyari et al. 2019). Recent paleoseismological and geomorphic studies suggest that the flat surface of GRK has significantly changed after the 1819 earthquake (Mw 7.8) in the Western Great Rann (Thakkar et al. 2012; Tyagi et al. 2012). The paleoseismic and archeological evidences suggest that the GRK likely experienced moderate to strong earthquakes in CE 893 and CE 1668 (Oldham 1883; Rajendran and Rajendran 2001). The archeological evidences from the Dholavira Harappan enclave, which was built on the upthrown block of the Island Belt Fault (IBF) ca. 4000 BCE, was destroyed by a major earthquake around 2200 BCE (Bisht 2011; Kothiyari et al. 2019).

Although Kachchh is an active intraplate seismic zone, the details of the precise tectonic behavior, uplift rates, and distribution of active deformation among the faults of the region are still obscure (Rajendran and Rajendran 1999 and 2001). Active faults are considered to be the source for large earthquakes in seismically active regions. Proper identification and distribution of these faults will significantly help in estimating the seismic potential and associated hazard in the region. Geomorphic evidence of active deformation has been reported from several locations within the Kachchh Rift Basin (Mathew et al. 2006; Patidar et al. 2007; Patidar et al. 2008;

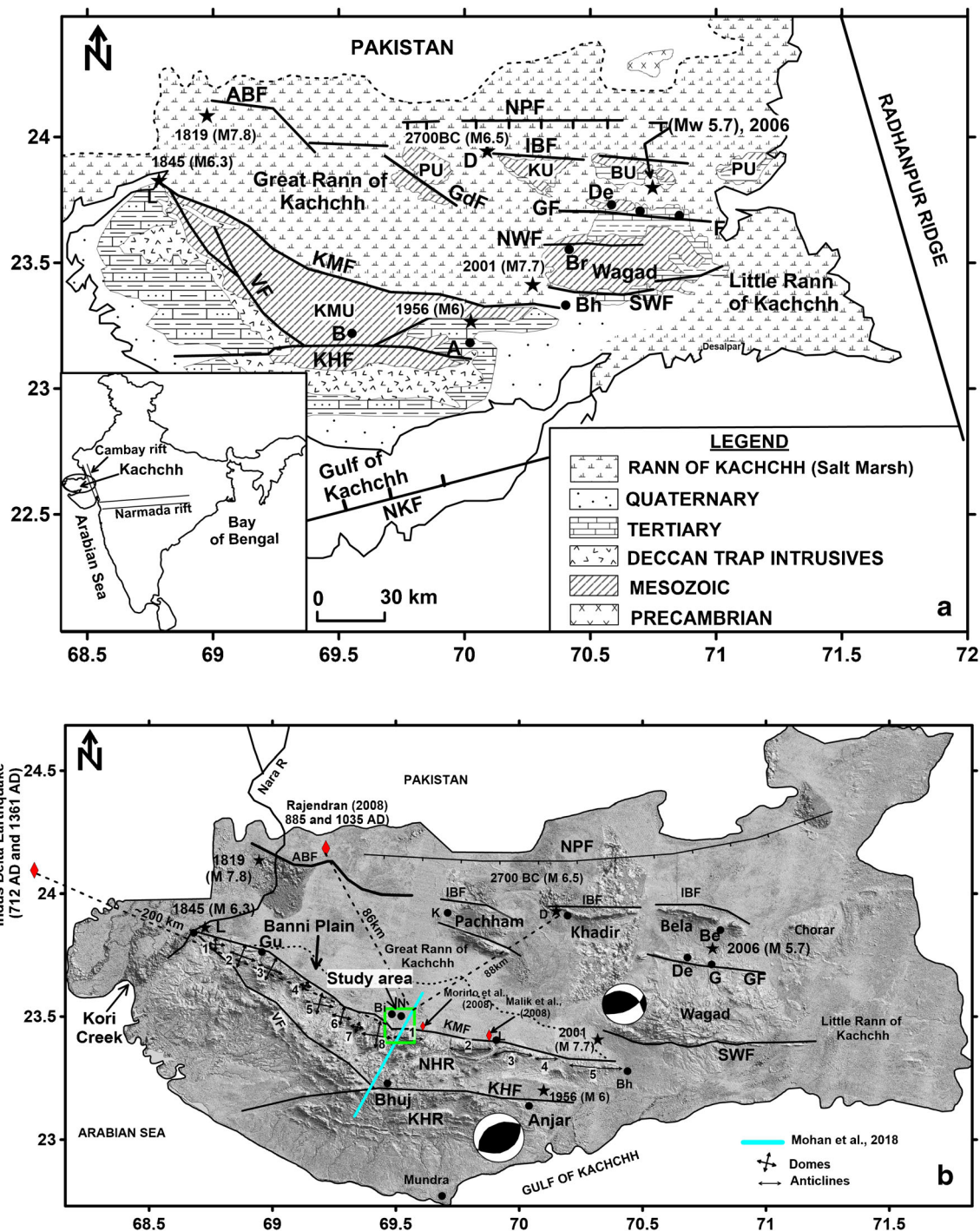


Fig. 1 (a) Seismotectonic map of the Kachchh rift basin integrated with the geological map, showing the epicenters of significant earthquakes (modified after Biswas 2005). **(b)** SRTM DEM of the Kachchh rift basin shows major morphotectonic features of the region and locations of major historic and recent earthquake events. Focal mechanisms of the 2001 Bhuj earthquake (Mw 7.7) and 1956 Anjar earthquake (Mw 6.0) are shown after Chung and Gao (1995) and Mandal et al. (2004). Fault lines: KHF (Katrol Hill Fault), KMF (Kachchh Mainland Fault), SWF (South Wagad Fault), GF (Gedi Fault), IBF (Island Belt Fault), ABF (Allah-Bund Fault), NPF (Nagar Parkar Fault). Uplifts: KHR (Katrol

Hill Range), NHR (Northern Hill Range), Locations: L (Lakhpat), Gu (Guneri), Bi (Bibar), N (Nirona), L (Lodai), Bh (Bhachau), De (Desalpar), G (Gedi), D (Dholavira), K (Khavda). Domes: 1. Lakhpat, 2. Guneri, 3. Jara, 4. Jumara, 5. Manjal, 6. Keera, 7. Chhari, 8. Dhardongar. Anticlines: 1. Jhurio, 2. Habo, 3. Kas, 4. Jhuran, 5. Kabrau. Location of present investigation is shown by the green rectangle, with distance from major historic earthquake marked by dashed black lines. NE-SW oriented solid cyan line indicates direction of MT profile (Mohan et al. 2018) Bronk Ramsey

Kundu et al. 2010; Chowksey et al. 2011; Kothiyari et al. 2016a, 2016b and 2016c). Along with the modern and historic earthquake records (Malik et al. 1999), active tectonic studies and a few paleoseismic investigations focusing mainly on paleo-liquefaction features suggest that the Kachchh region has remained under the influence of active tectonic movements during the historic and geological past (Sohoni et al. 1999; Sohoni and Malik 1998, Rajendran et al. 1998; Malik et al. 2001; Rajendran et al. 2001; Mathew et al. 2006; Kothiyari et al. 2016a and 2016b). The geomorphic and paleoseismic studies from intraplate Kachchh revealed that the major faults, viz., the Katrol Hill Fault (KHF), Kachchh Mainland Fault (KMF), South Wagad Fault (SWF), and Gedi Fault (GF) have ruptured the younger Holocene surfaces (Morino et al. 2008; Malik et al. 2008, 2017; Kundu et al. 2010; Kothiyari et al. 2016a, 2016b). However, no detailed field and paleoseismic investigations have been carried out in the central portion of KMF. So far, limited paleoseismic information is available from the eastern portion of the KMF (Malik et al. 2008; Morino et al. 2008). Therefore, we emphasized our studies along the KMF, with an aim to identify evidence for active faults, and signatures of paleoseismic events that occurred along KMF. Considering the fault activity based on previous works (Malik et al. 2008; Morino et al. 2008; Mathew et al. 2006), we examined the satellite data and carried out detailed field investigation along the central segment of the KMF. We identified signatures of an active fault that ruptured recent sediments along a north-dipping fault plane which is well supported by the published results of Mohan et al. (2018) and Gayatri et al. (2018).

In this study, we present the first exposure of the north-dipping active fault from two trenches opened across the active fault traces between Bihar and Nirona villages along the KMF (Fig. 1b). We report signatures of four paleo-earthquakes that occurred between 8300 and 890 years along KMF. The most recent earthquake has occurred between 1300 and 890 years. Further, the study revealed that these events are one of the possible factors responsible for the abandonment of Harappan civilizations.

Generalized Geology, Tectonic Setup and Geomorphology

The mainland zone of Kachchh constitutes a rocky terrain having broadly sub-parallel E-W trending hill ranges known as Northern Hill Range (NHR) (Biswas 2005). The NHR is bordered by the plain of Quaternary sediments Banni and GRK in the north and flat upland areas in the south. The upland areas comprise a chain of domes of Jurassic and Cretaceous rocks. Folded rocks of Mesozoic age are exposed

as domes and asymmetrical anticlines that occur south of KMF (Chowksey et al. 2011, Mathew et al. 2006). Lower Cretaceous rocks are present only in the southern slopes of the Mainland overlain by Deccan Trap volcanic flows and eastward on-lapping Neogene strata (Kothiyari et al. 2016b). North-flowing rivers originate from the northern flank of the Katrol Hill range cut across the KMF and emerge in the Banni Plain fans (Fig. 1b).

The KRB comprises the presence of Mesozoic, and Cenozoic sedimentary succession (Biswas 1993). The basin is bounded between two major faults such as NPF to the north and the North Kathiawar Fault (NKF) to its south (Fig. 1b). Along with these faults, the Kachchh is characterized by several E-W striking intra-basinal normal faults (Biswas 1987). These faults were initially developed as a peri-cratonic rift during the breakup of Gondwana land in Late Triassic (Biswas 1987). The tectonic episodes and stress reorientation of these faults took place in three phases: (1) post breakup: lithospheric rebound and trailing edge uplift—vertical displacement along reactivated faults; (2) drift stage: mainly horizontal stress—transtensional strike-slip movement; and (3) post-collision: convergence—horizontal stress—strike-slip movement (Gowd et al. 1992; Biswas 1993, 2005, 2016; Biswas and Khattri 2002; Biswas 1977, 1987; Rastogi et al. 2014; Kothiyari et al. 2016c).

The KRB is occupied by five major E-W oriented geomorphic zones, starting from south (a) the coastal zone, demarcates the southern boundary of the basin, (b) central rocky upland of Mainland Kachchh, (c) Banni grassland located to the north of Mainland region, (d) chain of island such as Pachham, Khadir, Bela, and Chorar, and (e) the Great Rann of Kachchh (Biswas 1987; Malik et al. 2017). In other words, the landscape of the Kachchh Basin is characterized by highlands surrounded by lowlands (Fig. 1b). The highlands are tilted uplifts along E-W trending faults and lowlands are intervening sediment filled half grabens (Biswas 2005; Kothiyari et al. 2019). The highlands are hilly terrains with peripheral coastal plains and the intervening lows are extensive mud and salt flats (Rann of Kachchh). Structurally, these geomorphic zones are controlled by major E-W faults (Biswas 1993, 2016). The KHF marks a boundary between the Katrol Hill range and the Bhuj low; in the KMF zone, the Northern Hill range abuts against the Banni Plain, and the E-W oriented IBF marked by the chain of islands (Biswas 1993; Malik et al. 2017). The Gulf of Kachchh, Banni grassland, and the Great Rann of Kachchh are the major structural lows. In the east of the Mainland, the Gulf of Kachchh shallows eastward into the mudflat named the Little Rann of Kachchh, between Wagad and the Kathiawar highland (Kothiyari et al. 2019). The morphological expression of deformation pattern along these faults is attributed by the presence of steeply north-dipping uplifted scarp and a gentle back slope produced by wrench faults (Biswas 2016; Kothiyari et al. 2016a, b, c, 2018).

The KMF is an E-W oriented ~ 160 km long morphogenic structure forming steeply north dipping 40 to 100 m high scarps in the anticlinally folded NHR (Maurya et al. 2003). Several structurally controlled domes (Lakhpat, Karanpar, Guneri, Jara, Jhumara, Nara, Manjal, Keera, Dhar Dungar) and anticlines (Mundhan, Jhurio, Habo, Kas, Jhuran, and Khirasara) of various dimensions are associated with KMF (Fig. 1b). The northern ends of these domes and anticlines are suddenly truncated along the KMF and form a steep north-facing escarpment. The domes associated with the KMF are circular in shape. The experimental model of Withjack and Scheiner (1982) suggests that the circular domes are developed on the crest and along the flank of a normal fault with shallow deformation with or without a simultaneously applied regional horizontal strain. Strike-slip faults oriented NE-SW may generate sufficient compression strain on the flanks of the main fault, to produce the circular domes in the area.

Historic earthquakes in the Kachchh region of Western India

The Mesozoic tectonic events in Kachchh Rift Basin were initiated during the breakup of Gondwanaland and the northward drift of the Indian plate (Rajendran and Rajendran 2001). The rift basin that evolved as a consequence of this breakup was controlled by a series of normal faults (Biswas 2005). The movement along these faults produced several earthquakes in the recent past, as indicated by the fault plane solutions of other rift-related earthquakes in Peninsular India (Talwani and Gangopadhyay 2001; Chung and Gao 1995; Rajendran and Rajendran 1999, 2001; Malik et al. 2017; Kothiyari et al. 2016a, b, c, 2018, 2019; Biswas 2016). However, no reliable information on significant pre-1819 earthquakes is available, though an event is reported to have occurred in 1668 (Burnes 1835, Rajendran and Rajendran 2001) (Fig. 1b). A significant post-1819 earthquake event might have occurred in 1844 or 1845 (Jacob 1860; Wynne 1872; Rajendran and Rajendran 2001). Nelson (1846) and Jacob (1860) reported that the Kori Creek was flooded, and the ground was uplifted by 1 m during multiple earthquake events during this time (Bilham 1998). However, there is no historical evidence of location, size, and time of these major historical earthquakes (Rajendran and Rajendran 2001). The 1956 Anjar (M 6.1) earthquake that killed 115 people and injured hundreds is a moderate event in the post instrumentation era. This earthquake is believed to have occurred along the eastern edge of the KMF. The fault plane solution of the 1956 earthquake indicates reverse faulting on an NE-SW oriented plane dipping (45°) northward (Chung and Gao 1995) (Fig. 1b). However,

there is no surface deformation reported from the 1956 Anjar earthquake event, and the nodal planes have the same orientation as the 1819 scarp. Based on these observations, Chung and Gao (1995) postulated that both these earthquakes might have been triggered in the same stress field (Rajendran and Rajendran 2001).

The 1819 main shock occurred on 16 June at around 6:50 p.m. and lasted for about 2 min (Mac Murdo 1824; Bilham, 1998; Rajendran and Rajendran 2001). The strongly affected area was confined to a 300-km radius, nearly 7000 houses were destroyed at Bhuj, and more than 1150 people were buried in the ruins (Rajendran and Rajendran 2001). The report by Mac Murdo (1824) suggests that during initial shaking of the 1819 earthquake, the ground motion was vertical, while the later motion was undulatory and widespread liquefaction has been observed. The earthquake caused significant changes in the fluvial systems. The Nara River (a tributary of Kori Creek) was dammed, forming a pond; as a result, the downstream part of the river dried up after the earthquake (Glennie and Evans 1976). Ground uplift was the most remarkable feature developed during the 1819 earthquake. During the earthquake, a part of the Great Rann of Kachchh was uplifted and the approximately 90 km long Allah Bund fault scarp was developed (Rajendran and Rajendran 2001).

Geometry of Kachchh Mainland Fault

The KMF is the longest fault in the Kachchh Rift Basin extending ~ 160 km from the northwestern corner of mainland near Lakhpat to Bhachau in the east. Geometrically, the KMF evolved within the peri-cratonic rift basin was primarily reactivated as normal fault during rift stage when the vertical stress was dominating, and later, horizontal stress developed and flower structure related to strike-slip faulting were evolved during inversion stage (Biswas 2016; Fig. 2), as evident from the present structural and geomorphic pattern (Biswas 2016; Kothiyari et al. 2016c). Geomorphologically, the KMF is attributed by the presence of escarpments and hogback ridges of Mesozoic rocks facing Banni Plains to the north. The present-day structural pattern shows propagation of several second-order faults, exposed towards the footwall block collectively generating a 2–5 km wide KMF zone, as evident from an echelon placement of stratigraphic and structural units (Fig. 2). Towards the eastern end of the fault, an overlap zone (extensional step over; Samakhiali graben) is developed. Furthermore, in the central portion of KMF, another step over (contractional) is located close to Jhurio, where positive flower structure is well exposed (Biswas 2005). Similarly, several branches of KMF are interacting together at Nirona locality and making a positive flower structure. Some of these fault branches are dipping north and some are

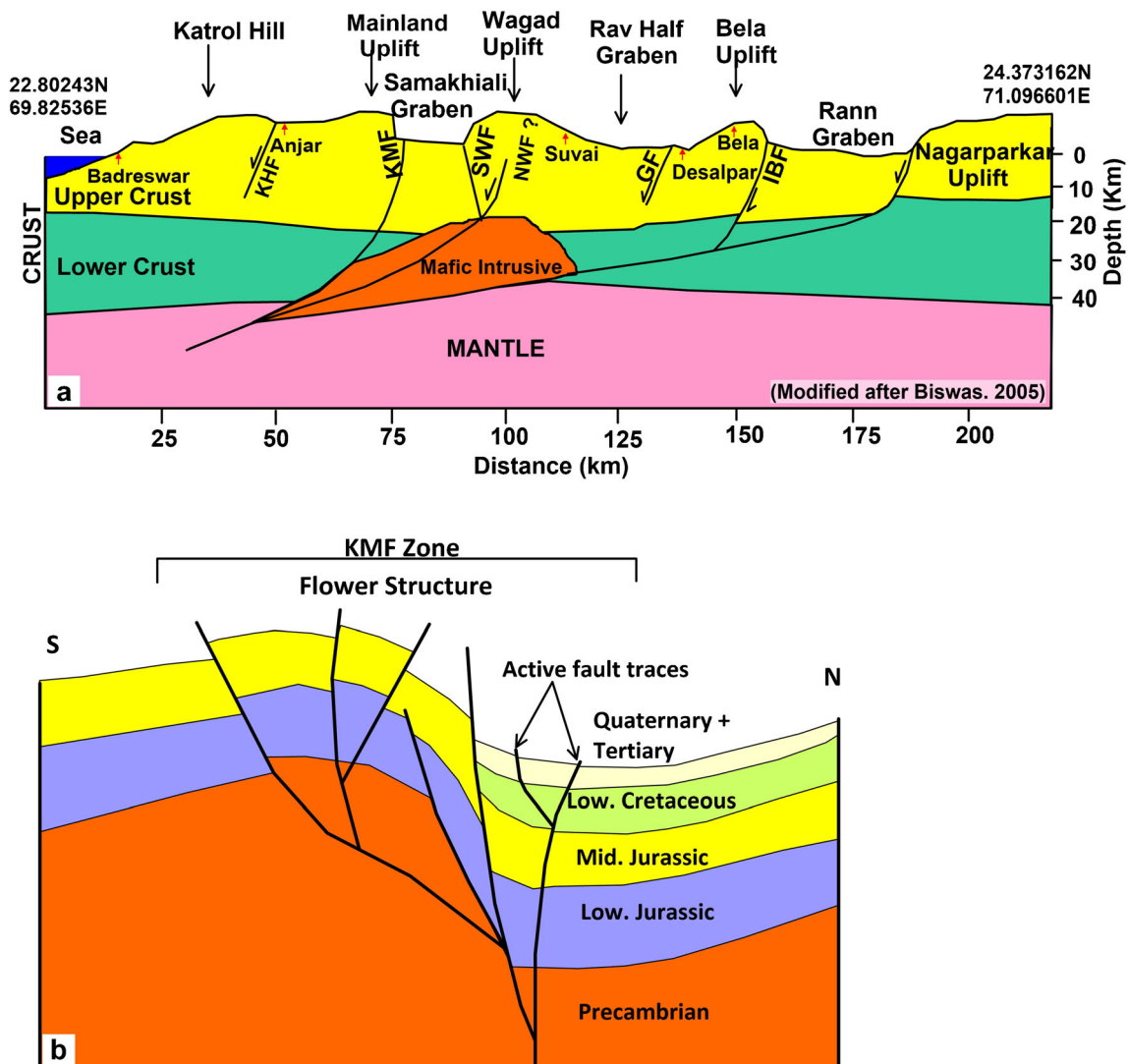


Fig. 2 (a) Conceptual geological cross section of the Kachchh region (after Biswas 2016). (b) Schematic representation of flower structure in the central KMF zone shows traces of active fault

dipping towards south. The south-dipping branches are hidden below the Quaternary cover.

The geological observation carried out along the fault zone suggests that the fault is gently dipping towards the north (Biswas 2005, 2016). The KMF is marked by a zone of second-order subsidiary faults' presence parallel to the foot of the escarpment where vertically north-dipping Tertiary beds are juxtaposed with steeply down-folded Mesozoic beds (Biswas 2016). Within the fault zone, slicken sided surface between Mesozoic and Tertiary rocks and brecciated purple ferruginous quartzite ridges are well exposed (Biswas 2016). The fault plane is nearly vertical and strikes WNW-ESE in the western part and strikes E-W in the eastern part. Towards the western part, the fault dips 80° to 85° towards the south; in the central portion, it dips 75° – 85° towards the north, and in the eastern part, the fault is dipping by 70° – 80° to the north.

The 2D seismic profile by ONGC confirms the vertical attitude of the fault in the subsurface (Biswas 2016). The KMF is dissected by several conjugate synthetic/antithetic faults meet the main fault at acute and/or high angles and makes an anastomosing rupture pattern of Riedel faults (Biswas 2016; Kothiyari et al. 2016c; Wilcox et al. 1973). The overlapping zones of fault segments show changing dip and strike, co-existence of faults with normal and reverse separation thus making a narrow linear or curvilinear deformation zone (Wilcox et al. 1973; Christie-Blick and Biddle 1985; Kothiyari et al. 2016c). Globally also, it is observed that the transverse faults are responsible for the change in the dip direction as in the San Andreas Fault system in Southern California (Nicholson et al. 1986), the Lake Mead fault system in the Basin and Range province (Ron et al. 1986) and the Alpine Fault system in New Zealand (Lamb 1989). Based on

the Bouguer gravity anomaly pattern, Chandrasekhar and Mishra (2002) suggested that the KMF is a near vertical fault. The seismological fault plane solution data of Rastogi et al. (2014) suggested the KMF as a south-dipping fault. However, analysis of earthquake in the epicentral zone 2001 Bhuj earthquake carried out by Mandal (2016) reveals that the fault dip towards the north. Similarly, the geological and shallow subsurface geophysical investigation of Joshi et al. (2012) using ground penetrating radar (GPR) across the KMF suggested it as a north-dipping normal fault. Further, the GPR survey carried out by Maurya et al. (2016) shows that the KMF as a near vertical north-dipping fault tends to become steep southward-dipping fault in the vicinity of transverse faults. Further, the paleoseismological investigation by Morino et al. (2008) and Malik et al. (2008) in the eastern part of the KMF zone suggests that the KMF is a low to high-angle south-dipping fault. Based on trench stratigraphy, Malik et al. (2008) identified three fault strands: F1 dips 55° towards the south, F2 dips 30–40° towards the south, and the F3 dips by 10° towards the south. The magnetotelluric (MT) studies by Naganjaneyulu et al. (2010a) suggested the lithounits within the KMF zone are southerly dipping. Similarly, the MT investigation by Mohan et al. (2010) reveals that the KMF is a south-dipping thrust fault. Furthermore, Chandrasekhar et al. (2012) identified an E-W trending south-dipping reverse fault close to KMF. Interestingly, the magnetotelluric survey carried out by Sastry et al. (2008) shows the presence of KMF in the area but they have not described the geometry, but the resistivity profile acquired by Sastry et al. (2008) clearly shows steep north-dipping resistivity contrast. Sarkar et al. (2007) carried out a seismic survey which shows that the KMF is a south-dipping fault. Further based on the magnetotelluric investigation by Mohan et al. 2018 in the central portion of KMF zone, it suggests the KMF is north-dipping normal fault. It has been argued that the transverse across the KMF plays an important role in changing the dip direction; the locations of geophysical and geological investigation carried out by Sarkar et al. (2007), Morino et al. (2008), Malik et al. (2008), Mohan et al. (2010), and Rastogi et al. (2014) are located close to the transverse fault and hence show southerly dip of the fault.

Recently, Mohan et al. (2018) acquired ~ 55 km long N-S profile of MT between Jiyapar and Sherov localities (Fig. 3a). The MT profile clearly shows the presence of a north-facing conductive zone with low resistivity between the stations 7 and 10 south of Nirona village. This low resistive zone is interpreted as a north-dipping KMF (Mohan et al. 2018) which is well correlated with the existing topography.

The topography plotted against an interpreted model of Mohan et al. (2018) clearly shows the presence of north heading fault scarp south of Nirona village (Fig. 3b). The geological investigation carried out in present study shows the presence of anticlinal structure in the area. The forelimb of the anticline

dips 75° towards N and forms a north-facing fault scarp of the KMF. Along the surface trace of fault, E-W oriented discontinuous linear mounds (pressure ridges) are observed along the trace of the KMF. These linear mounds could be developed as a result of the manifestation of the displacement along KMF. Further, in the central portion of MT profile, a vertical conductor up to 20 km depth is observed between Ulat and Kotda localities. Based on this vertical conductor, Mohan et al. (2018) inferred a new fault south of KMF and named as Ulat-Kotda Fault (UKF) (Fig. 3a). The geological investigation in the central part of the profile (within the zone of inferred fault) has been carried out to verify the location of fault. Our field investigation shows that the Mesozoic strata displaced along a steeply south-dipping (75–80°) normal fault. In the MT profile, a steep south-dipping conductive zone has been observed between Manjal and Jiyapar locations which are correlated with the location of the Katrol Hill Fault (KHF; Mohan et al. 2018).

Methodology

We mapped geomorphic surfaces using CARTOSAT-1 imagery downloaded from the National Remote Sensing Centre/ Indian Space Research Organization (NRSC/ISRO) web site (<http://bhuvan.nrsc.gov.in/data/download/index.php>) and SOI topographic maps (1:50,000 scale). The data were processed using the Global Mapper-16 software in WGS 84 projection. The details of site location are illustrated in Fig. 4a. Surficial mapping and the results of optical dating are provided in Sections 5 and 6. We generated topographic profile across the fault scarp that offsets the youngest geomorphic surfaces. Trenches were then excavated across the active fault scarps preserved in Holocene alluvial/fluviol sediments. Trench exposures were logged to show the structural and stratigraphic relations used to determine the timing, geometry, and size of past earthquakes. Fault traces and stratigraphic contacts were logged in the field using a 1 × m grid system on the exposed faces depending on the amount of detail necessary to illustrate the stratigraphic contacts and fault traces. All measurements discussed in trench descriptions are in meters along the length of the trench from north to south, followed by depth in meters below to an arbitrary datum established near the top of the trench. The sediments observed in the trench exposure were differentiated as individual units on the basis of grain size, texture, color, bioturbation, lithology, and inferred depositional environment. These units are numbered in increasing order from youngest to oldest in the trench logs.

OSL Chronology

Samples for optically stimulated luminescence (OSL) dating were collected from the different stratigraphic horizons. At places, multiple samples were collected

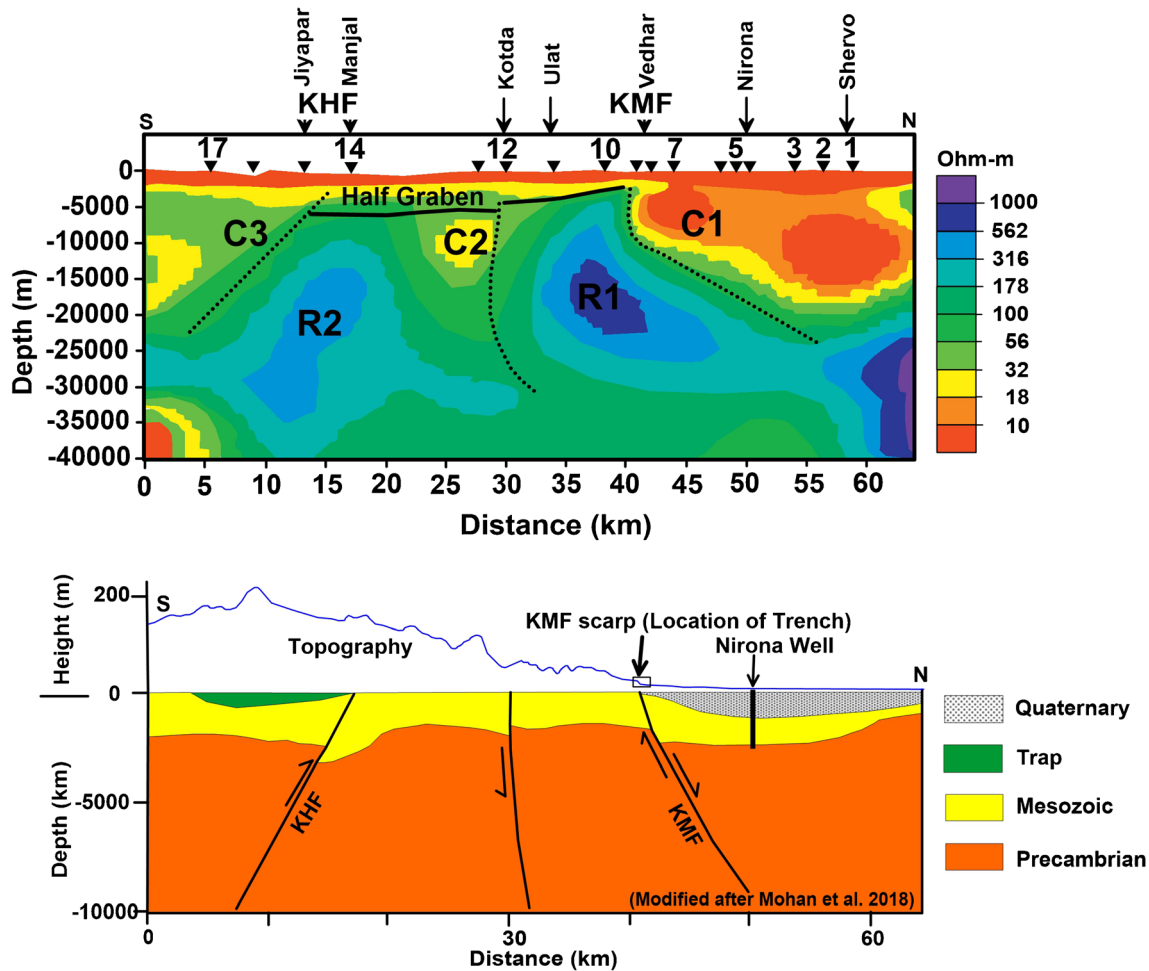


Fig. 3 N-S oriented approximately 65 km long magnetotelluric profile shows presence of sharp north dipping resistivity changes in the KMF zone. Below the interpreted depth profile shows offset of lithounits along

a north dipping fault (modified after Mohan et al. 2018). The topography against the fault is shown by blue line and the location of trench is marked by black rectangle

vertically from the alluvial sediment succession in order to check the temporal variability in sedimentation. The ages were obtained based on medium to coarse-grained quartz extract, using the single-aliquot regeneration (SAR) protocol of Murray and Wintle (2000) with preheat of 240 °C for 60 s and cut heat of 200 °C. Luminescence measurements were made using an automated Risø TL-OSL reader (TL/OSL-DA-20; Boetter-Jensen et al. 2003). The samples were stimulated using a blue diode (470 ± 20 nm). The detection optics comprises an EMI 9835QA photomultiplier tube coupled with a 7.5 mm Hoya U-340 filter (emission 330 ± 35 nm). Beta irradiations were carried out using an on-plate ⁹⁰Sr/⁹⁰Y beta source with a dose rate of 0.131 Gy/s. The OSL was measured at 125 °C for 40 s prior to every OSL measurement; infrared stimulated luminescence (IRSL) was measured at 50 °C for 100 s to remove any contribution from feldspar. The growth curves were constructed using five regeneration dose points including one point to estimate the recuperation and another point to estimate the reliability of

sensitivity correction (recycling ratio). The recuperation was < 1% of the natural signal and only those aliquots in which the recycling ratios were within 10% of unity were considered for age estimation. In samples where the over-dispersion (OD) value was > 40%, the minimum age model (MAM) is employed (Arnold et al. 2009) whereas in samples having < 40% OD, we used the weighted mean (Bailey and Arnold 2006). The annual dose rate is estimated by measuring the U, Th, and K concentrations using X-ray fluorescence. The errors of measurement (both systematic and statistical uncertainties) are < 5%, average water content of 10 ± 5 % was used, and cosmic ray contributions in dose rate were

Fig. 4 (a) Topographic map of the study area. Note: contour lines are marked by grey lines with a contour interval of 20 m, elevation peaks are shown by black triangles, and transverse faults are shown by black solid lines. Trace of active fault is marked by red dotted line; double solid black lines indicates road. (b) Geomorphological map of study area showing major geomorphic and geologic units

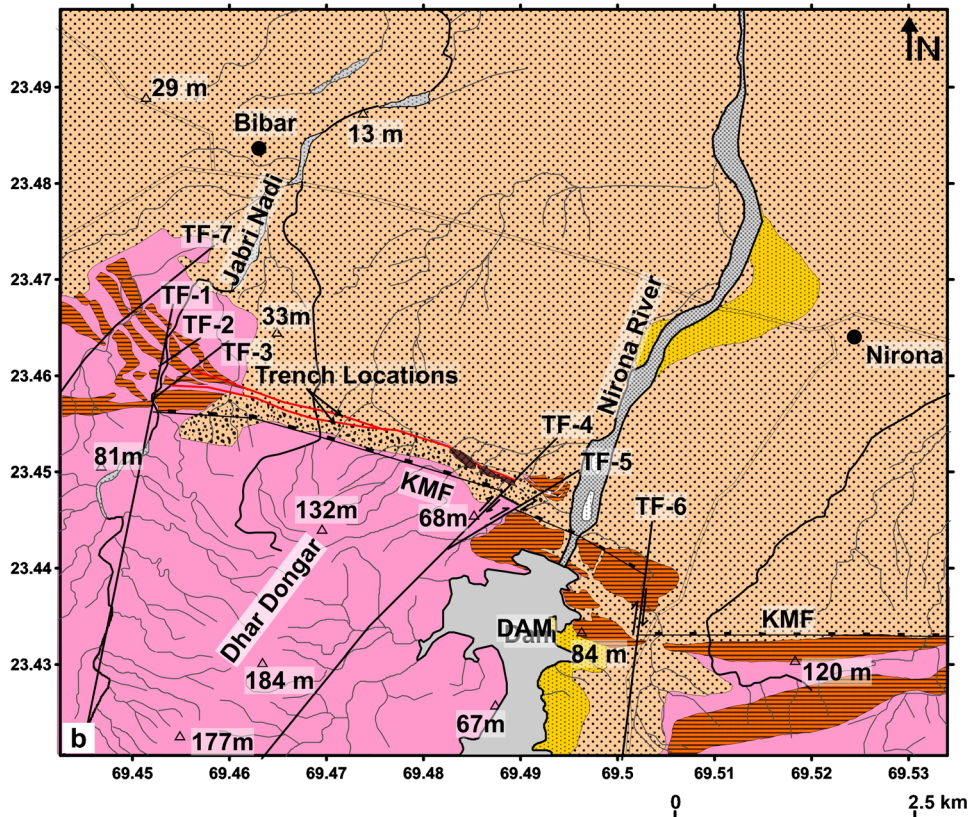
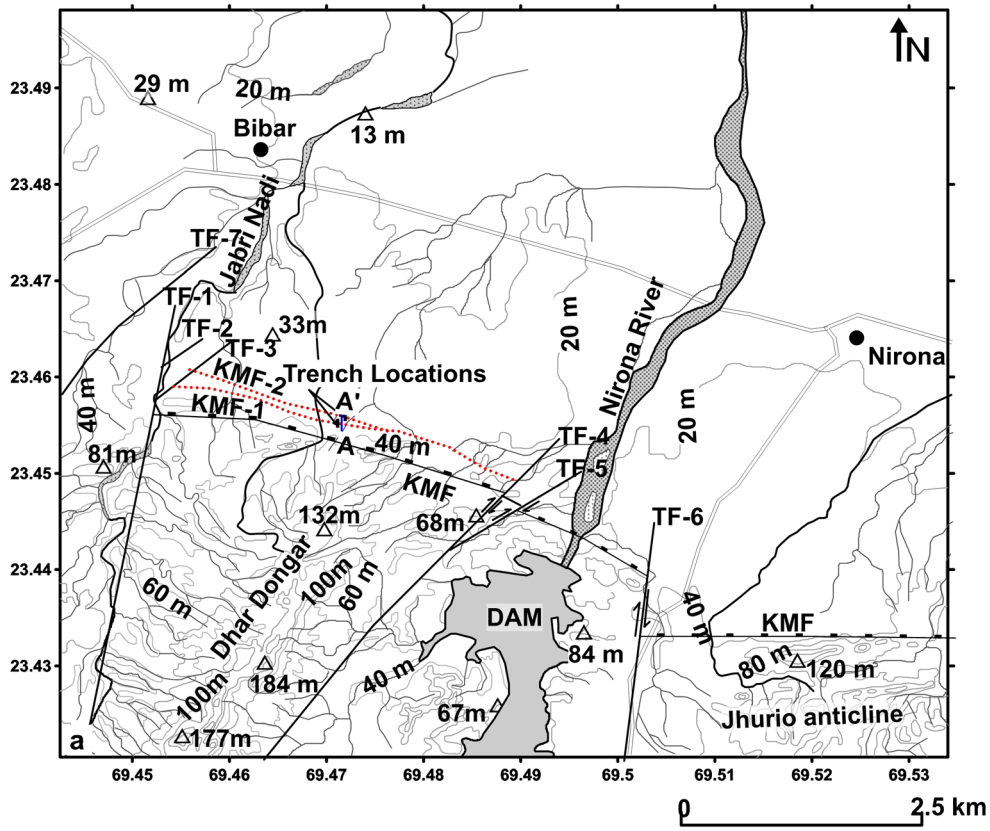


Table 1 Details of radioactivity and dose rate obtained using the single-aliquot regeneration methods. Palaeodose and ages obtained using the MAM and CAM method. OD represents discrepancy in DE data

Location	Sample	U (ppm)	Th (ppm)	<i>K</i> (%)	Dose rate (Gy/ka)	Palaeodose (Gy)	OD (%)	Age (ka)
Nirona	NIR-1	0.9 ± 0.04	8.6 ± 0.43	0.57 ± 0.03	1.4 ± 0.1	2.92 ± 0.54	90.2	2 ± 0.1
	NIR-2	1 ± 0.05	13.1 ± 0.65	0.46 ± 0.02	1.6 ± 0.1	1.75 ± 0.14	86.8	1 ± 0.1
	NIR-3	1.3 ± 0.06	9.3 ± 0.46	0.98 ± 0.04	1.9 ± 0.1	92 ± 1.9	22.89	48 ± 3.5
	NIR-4	1.1 ± 0.05	13.5 ± 0.67	0.40 ± 0.02	1.6 ± 0.2	27.6 ± 1.83	48.43	17 ± 1.6
	NIR-5	0.8 ± 0.04	9.6 ± 0.48	0.34 ± 0.01	1.3 ± 0.09	6.62 ± 0.68	60.2	7.2 ± 0.5
	NIR-6	1.2 ± 0.06	9.5 ± 0.47	1 ± 0.05	1.9 ± 0.1	121.51 ± 4.9	42.15	34.4 ± 2.5

beyond measurement uncertainties; OD > 30% may indicate significant scatter due to depositional or post depositional process

calculated using the method suggested by Prescott and Stephan (1982). Details of the radioactivity, devalues, dose rate, and ages obtained are given in Tables 1 and 2. The results of OSL ages are re-analyzed by DRAC OSL calculator (Durcan et al. 2015) and obtained similar results. Furthermore, the OSL ages are calibrated using Oxcal v4.3.2 software (Bronk Ramsey 2017).

Morphometric indices

Globally, the morphometric indices are considered powerful tools to examine the connection between tectonics and drainage basin morphology (Bull & McFadden 1977, Keller and Pinter 1996, Burbank and Anderson 2001; Harbor and Gunnell 2007; Kale & Shejwalkar 2008; Kothyari, 2015; Kothyari et al., 2016 a, b and 2018a). To evaluate these indices, we used Survey of India (SOI) topographic maps at the scales of 1:50,000 and CARTOSAT-1(2.5 m resolution) data is found suitable for regional scale morphometric analysis. The SOI topographic maps are geo-referenced with the help of CARTOSAT-1 data on GIS platform. The longitudinal profile of Nirona River has been generated with the help of geo-referenced SOI topographic maps (1:50,000 scale) of 1966 and 1973. Two commonly used geomorphic indices of active tectonics such as stream length gradient (SL) index and steepness index (K_s) have been calculated along the longitudinal length of the river.

Stream length gradient index

SL index is used to infer gradient changes by stream power and rock erodibility (Hack 1973; Burbank and Anderson 2001). The gradient index is expressed as:

$$SL = (\Delta H / \Delta L) \times L$$

where ΔH is the difference between two altitudes, ΔL is the change in length, and L is the total channel length from the point of interest, where the index is being calculated, upstream to the highest point of the channel (Hack 1973). Abrupt changes in slope ($\Delta H / \Delta L$) and the SL index have proved to

be an excellent method to evaluate the ongoing processes of uplift/incision of terrain (Seeber and Gornitz 1983).

Steepness index

The landscape evolution of the tectonically active region is essentially regulated by endogenic (tectonic) and exogenic (climatic) processes (Pazzaglia 2013). The longitudinal river profile in the active region provides information towards the role of endogenic and exogenic processes that may be used to ascertain the fluvial response to terrain instability/stability (Pazzaglia 2013). In active regions, the first-order drainage pattern sets the rate of lowering of a landscape (Merritts et al. 1994; Snyder et al. 2000; Whipple 2004; Pazzaglia 2013). Therefore, the bedrock incision rate in such regions is dominantly controlled by tectonic and climatic processes. However, in an equilibrium condition, when the climate and the rate of uplift are uniform, the longitudinal profile of a river will be graded (Seeber and Gornitz, 1983). In steady-state condition, the rate of erosion is balanced by uplift and can be represented by a power law function, and subsequently used to estimate steepness index (Flint 1974; Goldrick and Bishop 2007; Whipple et al. 2013) to estimate the steepness index as follows:

$$S = K_s A^{-\theta}$$

where S is the local channel slope, A is the stream drainage area, K_s is the steepness index, and θ is the concavity. In tectonically stable regions, the value of K_s remains constant for a given stream and in the active regions, the K_s may change from one segment to another (Whipple et al. 2013). Therefore, changes in K_s can be used to ascertain the variation in the uplift (Fig. 5).

River response to tectonic activity

Longitudinal river profile

The north-flowing Nirona River originates at an elevation of 180 m from the Katrol Hill range and traverses through the

Table 2 Details of radioactivity and dose rate obtained using the single-aliquot regeneration methods. Palaeodose and ages obtained using the WM, MAM, and CAM method. OD represents discrepancy in DE data beyond measurement uncertainties; OD > 30% may indicate significant scatter due to depositional or post depositional process.

Location	Sample code	U (ppm)	Th (ppm)	K (%)	OD (%)	No. of aliquots	Dose rate (ka)	Palaeodose (Gy)			Ages (ka)			Final age (years)	
								WM	MAM	CAM	WM	MAM	CAM		
Nirona trench 1 (23° 27' 14.91" N–69° 28' 15.03" E)	BBR2	1.1 ± 0.05	12.7 ± 0.63	0.81 ± 0.04	30.94	21	1.9 ± 0.1	16 ± 0.1	16.44 ± 1.01	17.81 ± 0.64	8.2 ± 0.6	8.5 ± 0.8	9.1 ± 0.7	8200 ± 600	
	BBR3	1.1 ± 0.05	11.3 ± 0.6	0.85 ± 0.042	40.95	24	1.8 ± 0.13	9 ± 0.1	7.4 ± 0.63	9.7 ± 0.43	4.6 ± 0.3	3.9 ± 0.4	5.1 ± 0.4	3900 ± 400	
	BBR5	1.5 ± 0.07	11.2 ± 0.56	0.83 ± 0.041	44.45	21	1.8 ± 0.3	8 ± 0.1	6.3 ± 0.63	8.58 ± 0.44	4.1 ± 0.2	3.2 ± 0.4	4.4 ± 0.3	4400 ± 300	
	BBR7	1.1 ± 0.05	9.8 ± 0.49	0.82 ± 0.041	30.01	22	1.7 ± 0.1	12 ± 0.1	13.46 ± 0.64	14.59 ± 0.48	6.8 ± 0.5	7.7 ± 0.7	8.3 ± 0.7	8300 ± 700	
	BBR8	1.5 ± 0.07	11.3 ± 0.56	0.74 ± 0.037	26.35	18	1.9 ± 0.1	9 ± 0.1	7.92 ± 0.42	8.08 ± 0.28	4.8 ± 0.3	4.2 ± 0.4	4.3 ± 0.3	4300 ± 300	
	BBR9	1.4 ± 0.07	15.5 ± 0.77	0.78 ± 0.039	29.77	26	2.1 ± 0.1	11 ± 0.1	10.91 ± 0.56	11.82 ± 0.36	5 ± 0.3	5 ± 0.4	5.5 ± 0.4	5500 ± 400	
	BBR10	1.2 ± 0.06	11.6 ± 0.58	0.82 ± 0.041	60.95	19	1.9 ± 0.1	11 ± 0.1	9.58 ± 0.51	10.49 ± 0.27	5.8 ± 0.4	5 ± 0.4	5.5 ± 0.4	5000 ± 400	
	BBR11	1.4 ± 0.07	11.1 ± 0.55	0.86 ± 0.043	57.78	18	1.9 ± 0.1	12 ± 0.1	9.12 ± 0.88	16.28 ± 1.16	6.1 ± 0.4	4.7 ± 0.5	8.3 ± 0.8	8300 ± 800	
	BBR13	1.5 ± 0.07	12.3 ± 0.61	0.85 ± 0.042	19.97	18	2 ± 0.1	6 ± 0.61	8.85 ± 0.45	9.58 ± 0.24	2.9 ± 0.3	4.4 ± 0.3	4.7 ± 0.3	2900 ± 300	
	BBR14	1.2 ± 0.06	12.8 ± 0.64	0.79 ± 0.039	31.7	20	1.9 ± 0.1	12 ± 0.1	11.59 ± 0.77	1.74 ± 0.08	6.1 ± 0.4	5.9 ± 0.6	0.89 ± 0.07	890 ± 70	
	Nirona trench 2 (23° 27' 21.75" N–69° 28' 20.14" E)	BBRT1	1.7 ± 0.0855	15.4 ± 0.77	0.78 ± 0.039	81	16	2.2 ± 0.1	4 ± 0.1	2.61 ± 0.31	6.69 ± 0.61	1.8 ± 0.1	1.2 ± 0.1	3 ± 0.5	1800 ± 100
		BBRT2	1.5 ± 0.075	14.2 ± 0.71	0.83 ± 0.0415	84.4	18	2.1 ± 0.1	10 ± 0.2	5.58 ± 0.37	17.64 ± 1.75	4.6 ± 0.3	2.6 ± 0.2	8.2 ± 1	4600 ± 300
		BBRT3	2.1 ± 0.105	15 ± 0.75	0.86 ± 0.043	62	23	2.3 ± 0.1	21 ± 0.3	13.33 ± 1.33	25.28 ± 1.74	8.9 ± 0.7	5.6 ± 0.7	10 ± 1	5600 ± 700
		BBRT4	1.9 ± 0.095	15.1 ± 0.755	0.88 ± 0.044	75	23	2.3 ± 0.1	14 ± 0.3	10.59 ± 1.32	27.11 ± 2.49	6 ± 0.4	4.5 ± 0.6	11.6 ± 1.4	4500 ± 600
BBRT6		1.2 ± 0.06	13.1 ± 0.655	0.74 ± 0.037	65	24	1.9 ± 0.1	3 ± 0.0	2.53 ± 0.10	4.81 ± 0.36	1.6 ± 0.1	1.3 ± 0.7	2.4 ± 0.3	1300 ± 700	
BBRTS1		1.4 ± 0.07	14.5 ± 0.725	0.86 ± 0.043	81	24	2.1 ± 0.1	19 ± 0.4	12.06 ± 1.91	23.34 ± 2.14	8.7 ± 0.6	5.5 ± 0.9	10 ± 1.2	5500 ± 900	
Terrace section	BBRS2	1.3 ± 0.065	13.3 ± 0.665	0.78 ± 0.039	69.7	24	1.9 ± 0.1	35 ± 0.4	34.81 ± 4.09	45.15 ± 2.42	17.5 ± 1.2	17.4 ± 2.4	17400 ± 2400		

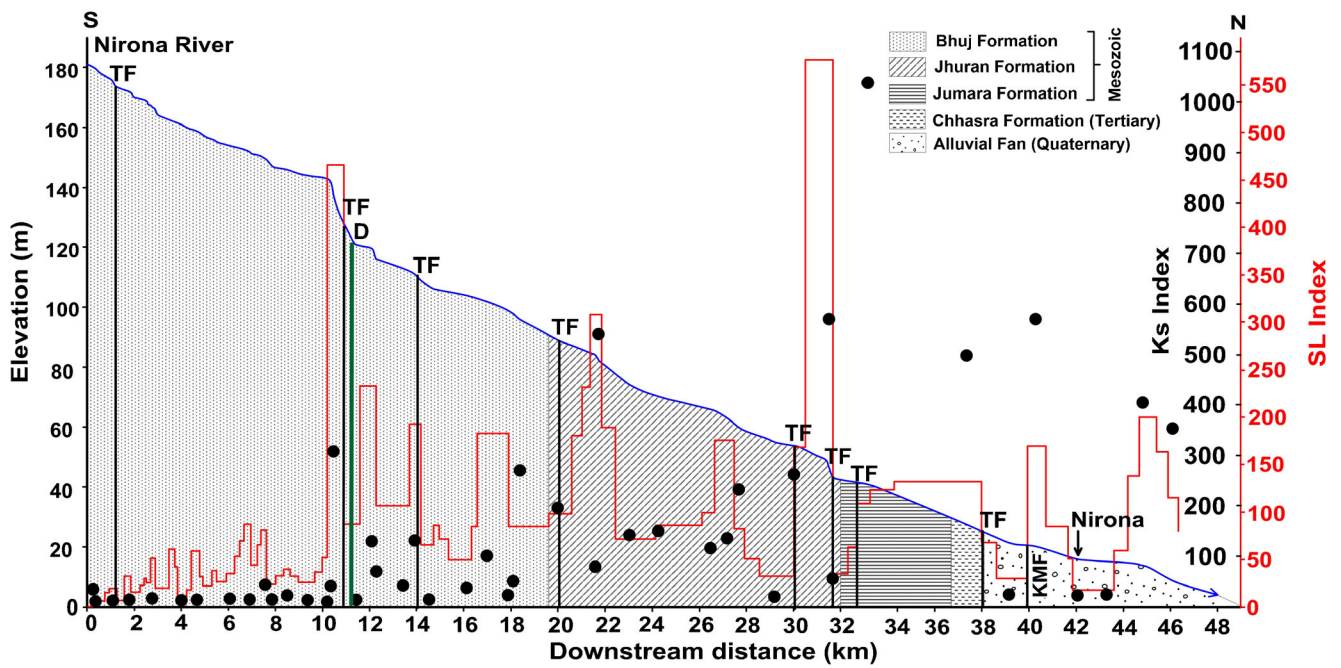


Fig. 5 Longitudinal profile of the Nirona River as it flows across the different geological units. The stream length gradient index (SL) is marked by red lines and steepness index (K_s) is marked by black filled circles. Faults are marked by black vertical lines; solid green line represents position of a dyke

sandstone, shale, and limestone of Mesozoic age in the upper and middle reaches (Fig. 5). However, towards the lower reaches, it traverses through calcareous limestone of Tertiary age and Quaternary alluvial sediments and terminates into the

Banni Plain at 4 m asl (Fig. 5). The 48 km long Nirona River flows across the structurally controlled lithology and cuts through several transverse faults (TF) towards the upper and middle reaches. These faults are reflected in the topography by

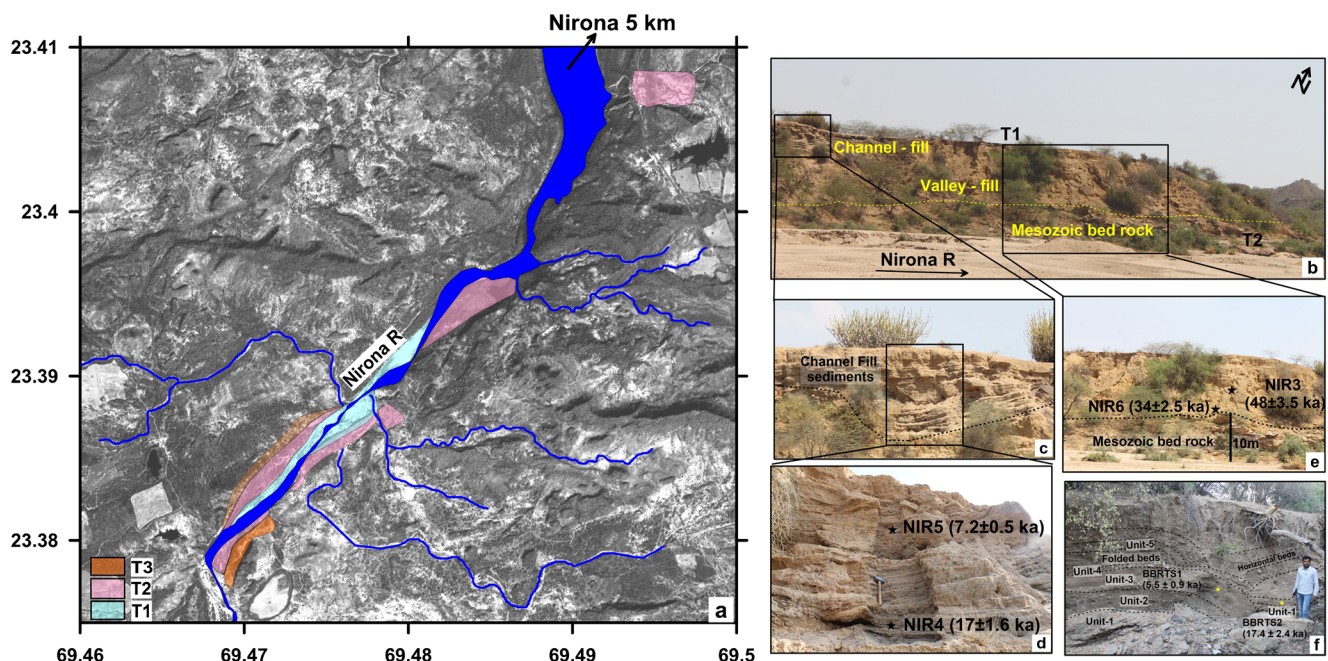


Fig. 6 (a) CARTOSAT-DEM generated topographic map of Nirona showing the locations of terraces; (b) field photograph of two levels of strath terraces, the upper terraces are fluvial strath terraces, the lower ones (T2) are rocky terraces, (c and d) texture and structure of channel fill sediments resting on top of terrace deposits (Kothyari et al. 2019). (e)

Configuration of valley fill sediments resting over a 10 m thick bedrock with a sharp aggradational contact. (Note: locations of sediments collected for optical dating are marked by black stars). (f) Deformed terrace stratigraphy close to the trench 2

the presence of knickpoints in the longitudinal profile of the river (Fig. 5). Downstream, it flows across the structural highs of Dhar Dungar dome and Jhurio anticline and incises the bedrock (Fig. 6). The river cuts through the KMF zone at the segment between 36 and 42 km where a sudden change in elevation is reported (Fig. 5). Two levels of 10 to 22 m thick incised unpaired strath terraces are observed in the segment between 32 and 34 km distance from the head of the river. Alluvial fans of considerable vertical thickness and lateral extent are observed downstream as the river leaves the KMF zone entering the plain of Banni, where no bedrock is exposed (Fig. 5). These alluvial fan surfaces are truncated along the active segment of the KMF.

SL and K_s index

We have calculated two conventional geomorphic parameters SL and K_s indices along the longitudinal length of the north-flowing Nirona River (Fig. 5). These indices are sensitive to any change in the river courses (Bull 1991; Keller and Pinter 1996; Goldrick and Bishop 2007; Whipple et al. 2013). The changes may highlight either the differential erosion of the bedrock due to the difference in lithologies or as a result of tectonic activity. For the computation of SL index of the Nirona River, a total river length of 49 km has been considered. The longitudinal profile reveals six prominent knickpoints at distances of 11 km, 12 km, 14 km, 22 km, 27 km, 32 km, and between 38 and 40 km where the gradient index values are also high (Fig. 5). The corresponding SL indices for these knickpoints are 460, 232, 188, 304, and 573 respectively that correspond to the presence of transverse faults. However, the higher SL values between 38 and 46 km are ranged between 250 and 375, which correspond to the activity associated with the KMF. The K_s indices for the Nirona River have been calculated and these values were plotted against the already calculated SL index (Fig. 5). Along the knickpoints, the observed values of K_s are 622, 128, 132, 196, 538, 569, and 1041, which are high and correspond to the activity associated with transverse faults (Fig. 5). However, the K_s values between 38 and 46 km are 499, 570, 404, and 353 which are high and correspond to the activity associated with the KMF.

Strath terraces

Fluvial strath terraces are another prominent geomorphic feature observed towards the hanging wall block of the KMF (Fig. 6a, b). Two levels of unpaired terraces were identified at 23° 23.819' N–69° 29.122' E (south of Nirona). Depending upon the ratio of the sediment and the vertical bedrock incision, these terraces are classified as strath terraces. The strath terraces are ~ 22.5 m thick, where ~ 8.7 m fluvial sediments are resting upon 10 m thick Mesozoic bedrock with a sharp

aggradational contact (Fig. 6b–e). These sediments are mainly composed of well-rounded to sub-rounded clasts of Mesozoic rocks with interspersed bands of medium to fine sand. They are capped by ~ 3.8 m thick cross-bedded channel sediments with a sharp aggradational contact (Fig. 6b–e). The channel sediments are made up of medium to coarse sand with dispersed gravels (Fig. 6c and e)

At the location 23° 27' 22.15" N and 69° 28' 20.93" E (close to trench 2), a 3.6 m thick set of alluvial fan deposits is observed. Based on the sediment texture and clast composition, five major stratigraphic units have been identified in the area (Fig. 6f). The oldest unit 1 is a clast-supported sub-rounded to rounded gravel unit with occasional sand lenses. Unit 1 is overlain by angular to sub-angular platy gravel unit 2, which is overlain by medium to fine laminated sand unit 3. The unit 3 is overlain by angular to sub-angular clast-supported gravels (unit 4). The unit 4 is overlain by clast-supported angular to sub-angular platy gravel unit 5 with occasional sand lenses. These stratigraphic units are highly deformed and folded along a monoclinical flexure. The forelimb of the fold is dipping 35° towards the north. However, the back limb is horizontally stratified in nature.

Timing of deformation

Optical ages of four samples from the Nirona section are shown in Table 1 and Fig. 6. The oldest sample collected from 3 m above the present-day river bed gave an OSL age of 13.7 ± 0.11 ka (NR-1). Two samples collected from 4.5 m and 6 m above the present-day river bed yielded an age of 8.4 ± 0.6 ka (NR-2) and 6.8 ± 0.57 ka (NR-3). However, the youngest sample collected from 10.5 m above the present-day river bed yielded an age of 5.7 ± 0.42 ka (NR-4) respectively. Based on the stratigraphic record, the present study shows two chronologically constrained tectonic uplift events. The older event is prior to 13 ka and the younger tectonic activity has occurred sometime during the last 5.7 ka.

Optical ages of samples (NIR-3, NIR-4, NIR-5, and NIR-6) collected from the older strath terraces are summarized in Fig. 6 and Table 1. Two samples collected from 10 m and 15 m above the present-day river bed yielded ages of 34 ± 2.5 ka (NIR-6) and 48 ± 3.5 ka (NIR-3), respectively. The age of NIR-3 is slightly overestimated, since in sediments, it should be younger than 34 ka. The samples collected from 20 m and 22 m above the present-day river bed yielded ages of 17 ± 1.6 ka (NIR-4) and 7.2 ± 0.5 ka (NIR-5), respectively. The chronological data suggests that the older valley fill sequence corresponding to the first phase of aggradation was deposited at ~ 34 ka and continued until around 17 ka. The second phase of aggradation took place after 7 ka. After the post, 7 ka deposition of sediments' major tectonic activity occurred due to the growth of a fault-related fold. This caused uplift of the bedrock with consequent incision of the river channel.

Based on the optical ages collected from the older strath terraces, the long-term incision/uplift rate was computed as 1.48 mm/year. Based on terrace surfaces and chronometric data, the oldest phase of mid-Holocene tectonic activity along KMF is bracketed between 5 and 7 ka.

Optical ages of samples (BBRTS1 and BBRTS2) collected from the oldest unit 1 and sand unit 3 are summarized in Fig. 6f and Table 2. A sample collected from the oldest unit 1 yielded an age of 17 ka, whereas sample collected from folded sand horizon gave an OSL age of 5.5 ka. Based on optical ages, the folding event is postdated to 5 ka.

Paleoseismic history of the KMF

The active fault traces of KMF striking E-W were inferred between west of Nirona and east of Bihar village. The position of the KMF is marked based on the topographic break between the northern hill range and the alluvial plain (Figs. 3, 4, and 7), representing a geographic domain boundary. Geomorphologically, the KMF is attributed by the presence of north-facing escarpments. As discussed previously, several parallel branches of KMF are interacting together at Nirona locality; some of these fault branches are dipping north and some are dipping towards the south. Based on detailed satellite data investigation and field survey, two traces of north-dipping KMF are identified in Holocene alluvial surface. Figure 4 shows the distribution of fault traces parallel and oblique to the KMF between Nirona and Bihar villages. The

active fault traces are marked based on the sudden truncation of alluvial fan surfaces approximately 150–300 m north of the morphotectonic scarp (Figs. 4 and 7). To confirm the active faulting and map the near subsurface displacement/deformation in Late Holocene deposits, we opened two trenches across the north-facing active fault scarp located between Nirona and Bihar villages (Figs. 4 and 7). For each site, we use structural, geomorphic, and paleoseismic data to highlight the characteristics of fault displacement along the KMF.

Structural pattern of the trench site

Structurally, the KMF segment between Nirona and Bihar is dislocated by several younger transverse faults numbered as TF-1 to TF-7 (Figs. 4 and 7). Based on the offset along local geological and geomorphic units, the net displacements along these faults have been estimated. The observed displacements along TF-1 to TF-7 are 200, 90, 72, 110, 100, 70, and 570 m respectively (Fig. 7). These NE-SW trending strike-slip faults dissect the domes and anticlines along the KMF (Fig. 7). The forelimb of the Mesozoic anticline dips 55° towards N and forms a north-facing fault scarp of the KMF, while the E-W oriented discontinuous linear mounds (pressure ridges) ranging in height from 10 to 20 m and 150 to 300 m long are observed along the trace of the active segment of the KMF (Fig. 7). These linear mounds could be developed as a result of the manifestation of the displacement along KMF and indicate

Fig. 7 (a) CARTOSAT satellite imagery of the study area showing traces of old geological fault and position of active fault. The Kachchh Mainland Fault is right laterally displaced by seven NE-SW oriented faults. The net apparent offset along these strike-slip faults are given in the top right corner. Locations of trenches are marked by solid black rectangles. Pressure ridges are highlighted by small yellow ellipses. Inset: Topographic profile of trench site

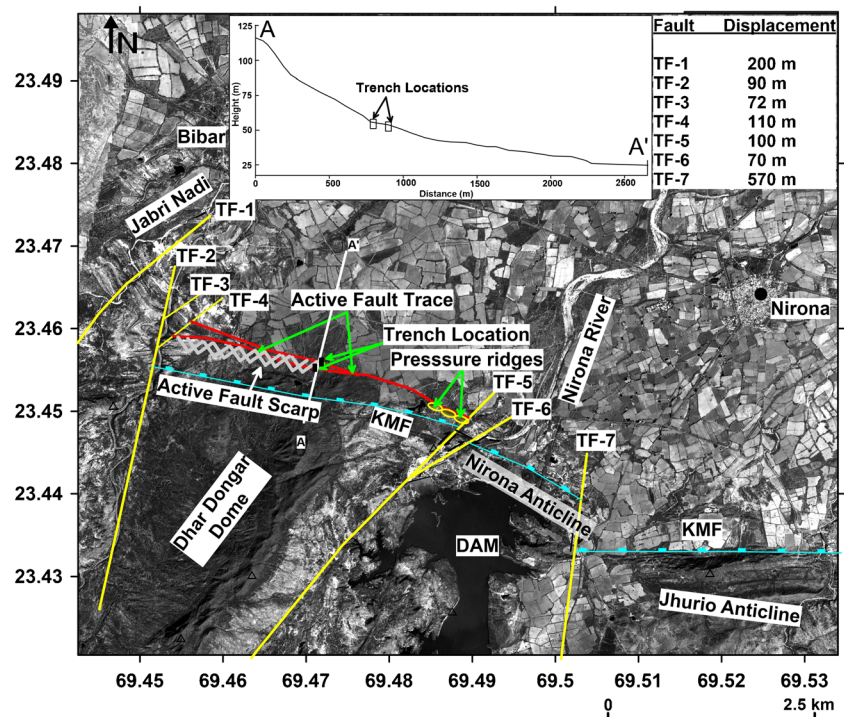




Fig. 8 Field photographs show (a) development of deep canyon toward the footwall block of KMF. (b) Sandstone and shale units displaced 1.5 m along a NE-SW oriented fault (c and d) uplift of river floor along the two

parallel normal faults and river ponding (e) offset of lithounits along a NE-SW oriented fault, and (f) north facing old geological scarp of KMF. The fault is dipping 55° northward

the progressive shift of tectonic activity towards the north along the newly developed imbricating strike-slip fault.

We observed a canyon-like incision around 1 km long and ~ 50 m wide along the north-flowing Nirona River within the faulted and dissected segment of the KMF (Fig. 8a). The sandstone and shale lithounits are found to be displaced by several small scales normal and NE-SW trending strike-slip faults with 1.5 m net slip. (Fig. 8b). Slickensides are observed on the ENE-WSW trending two parallel normal faults. The faults are dipping 75° and 68° towards southeast (Fig. 8c).

A trace of an NW-SE oriented normal fault dipping 68° NE has resulted in 3 m offset (Fig. 8d). Drainage offset and ponding are striking features observed within the faulted

blocks (Fig. 8 c and d). The Nirona River flows across the ENE-WSW trending faults. The active displacement along this fault has resulted in the blockage of the river channel towards the upthrown block of the fault, while river ponding has taken place towards the downthrown block because of the subsidence on the hanging wall (Fig. 8 c and d). In the south of Bibar (23° 27' 43.80" N, 69° 27' 28.45" E), a trace of NE-SW oriented 55° NW dipping fault is found and has displaced shale and calcareous sandstone that is exposed across the small streams (Fig. 8e). The north-dipping (55°) KMF scarp has been observed between 23.455653° N–69.468226° E and 23.458933° N–69.460360° E (Figs. 7 and 8f) and has been displaced by several NE-SW oriented faults (Fig. 7).

Geomorphology of the trench site

The KMF extends in the E-W direction for a length of 120 km from Lakhpat in the west to Bhachau in the east (Fig. 1b). The site is situated in the central part of the KMF that strikes E-W for a distance of about ~ 3.5 km across the map area (Figs. 4 and 7). The alluvial fan surface, offset by the KMF, is preserved between the Jabri and Nirona Rivers (Figs. 4 and 7). The morphology and sediment architecture of the alluvial fan aggradation suggest that the alluvial fans were deposited by two rivers. One of the strong reasons could be several phases of tectonic impulses in the hinterland that had generated the hill slope colluvium. The alluvial fan surface is truncated by the E-W trending KMF and delineated by a prominent north-facing scarp and offset of drainages (Figs. 4 and 7). In this section, initially, we have provided the geomorphic and geometrical expression of faulting on the surface and at the trench walls. Based on the stratigraphic and structural observations on the trench walls, the event stratigraphy is established, while the optical chronology sharpens interpretation adding the timing and size of the last surface rupturing related to a historical earthquake at the site.

Structural relationship

Within the overridden segments of strike-slip fault systems, imbricate fans of normal and thrust faults are commonly observed (Woodcock and Fisher 1986). In case of positive flowering, imbricate faults that splay converge upwards in the form of a duplex (Dahlstrom 1970; Kingma 1958; Lensen 1958). Such structures are usually bound by two continuous faults, containing small scale en echelon faults (Woodcock and Fisher 1986). The slip within the system is primarily controlled by localized geological units (Woodcock and Fisher 1986). Sometimes, the upthrusts follow a staircase like a trajectory within the heterogeneous geological strata (Ghosh 1993). The thrust cuts up-section along a *ramp* and then follows a horizontal zone parallel to the bedding (McCalpin and Carver 2009). Primarily, when the thrust develops in an undeformed sedimentary sequence, the flat is parallel to the bedding. Secondly, the thrust propagates upward direction from the brittle gravel to semi ductile sand; dip-slip movement occurred at an angle of the transport direction (Dahlstrom 1970) which is attributed in changes of deformation style (McCalpin and Carver 2009). A similar pattern of fault observed in a Nirona trench 1, where fault (F1) evolved during the first phase of earth movement. The F2 is a bedding parallel fault developed parallel to the bedding plane (gravel bed) and then propagates upwards through the sand layer due to bedding parallel shear strain.

Nirona trench 1 stratigraphy

The N-S oriented 2.4 m deep and 12 m long trench shows that six major units (units 1 to 6; oldest to youngest) which are identified on the basis of grain size, texture, color, and inferred depositional environment have been identified within the excavated west wall of the trench (Fig. 9). The oldest unit (unit 1) is weathered north-dipping Mesozoic bedrock which is overlain by (unit 2) sub-angular to sub-rounded clast-supported gravel bed with occasional sand lenses. The unit 2 is overlain by a medium to coarse sand (unit 3) with dispersed gravels. The thickness of these two units (units 2 and 3) varies from place to place. The units 2 and 3 are truncated and overridden by a north-dipping (~ 75° N) fault marked by F1 in Fig. 9b. The unit 2 and unit 3 are overlain by a thin, poorly sorted matrix-supported gravel unit 4, which is laterally well extended all along the trench wall (Fig. 9b). The matrix-supported gravel unit 4 is overlain by a clast-supported sub-angular to sub-rounded gravel (unit 5). The units 3, 4, and 5 are displaced along a north-dipping (33° N) fault marked by fault F2 in Fig. 9b and become horizontal within the unit 2. Finally, unit 5 is overlain by a thin cover of top gray sandy soil (unit 6).

Nirona trench 2 stratigraphy

The N-S oriented 2.5 m deep and 12 m long trench shows that major eight units (units 1 to 8; oldest to youngest), which are identified based on the grain size, texture, and color of sedimentary units, have been identified within the excavated west wall of trench 2 (Fig. 10). These stratigraphic units are horizontally stratified and uniform. The oldest unit (unit 1) is comprised of compact sub-angular to angular gravels. The matrix of unit 1 is bounded by calcareous material. The unit 1 is overlain by clast-supported gravel with occasional sand lenses (unit 2). The unit 2 is overlain by poorly sorted clast-supported angular to sub-angular gravels (unit 3). The units 1, 2, and 3 are displaced along a north-dipping (33° N) fault, marked by fault F in Fig. 10b. The unit 3 is overlain by clast-supported sub-rounded to sub-angular gravel (unit 4) with occasional sand lenses. The unit 4 is overlain by matrix-supported angular to sub-angular compact gravel (unit 5). This unit is overlain by clast-supported platy, sub-angular to sub-rounded gravel (unit 6). Calcareous sand dykes are the most striking features that are observed in the trench wall. These sand dykes (liquefaction products) are vertically injected through units 1–6 (Fig. 10). More commonly, these sand dykes are injected through the north-dipping fault and small secondary fracture during an earthquake event. Unit 7 is composed of sub-rounded to rounded clasts of channel fill deposits. Units 6 and 7 are overlain by clast-supported gravel unit with occasional sand lenses and sandy soil (unit 8).

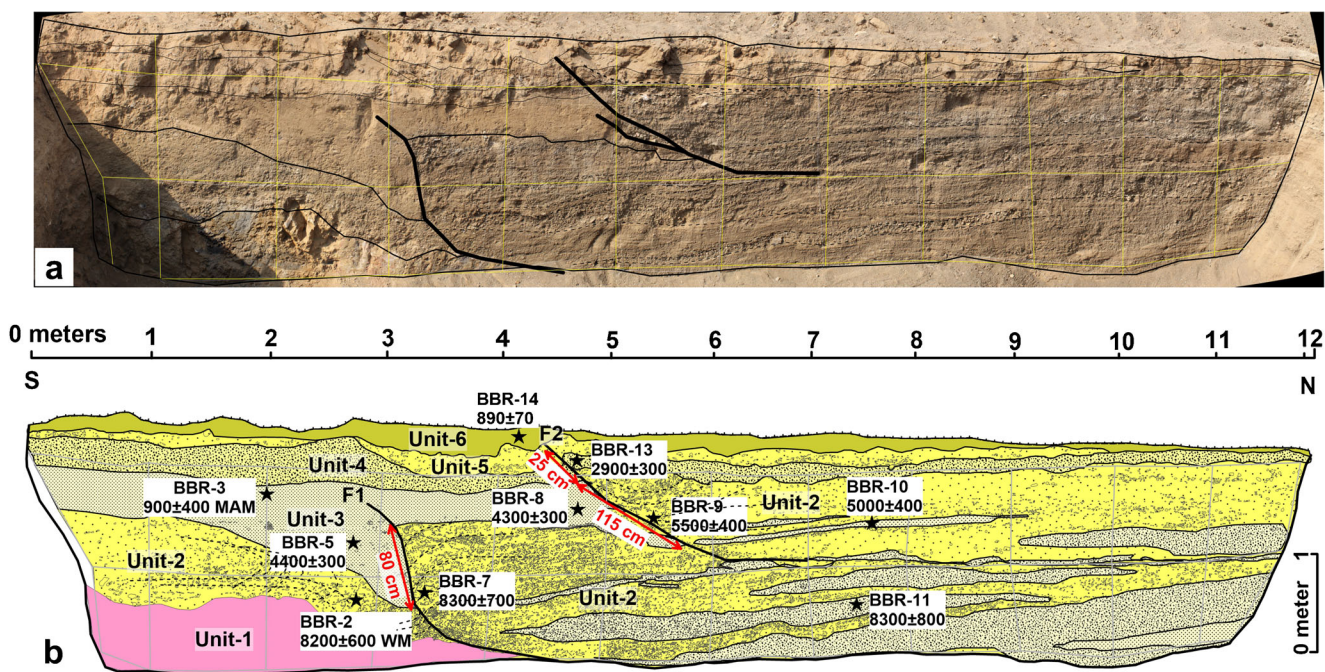


Fig. 9 (a) Photo mosaic of west wall of the trench excavated across KMF-1. Grids of 1 m × 1 m on a trench wall are marked by yellow lines; (b) log of the west wall of the trench. Six lithological units were

exposed. The oldest inferred earthquake, event I, displaced the oldest stratigraphic unit 2 along fault strand F1. Event II displaced units 2, 3, 4, and 5 along F2

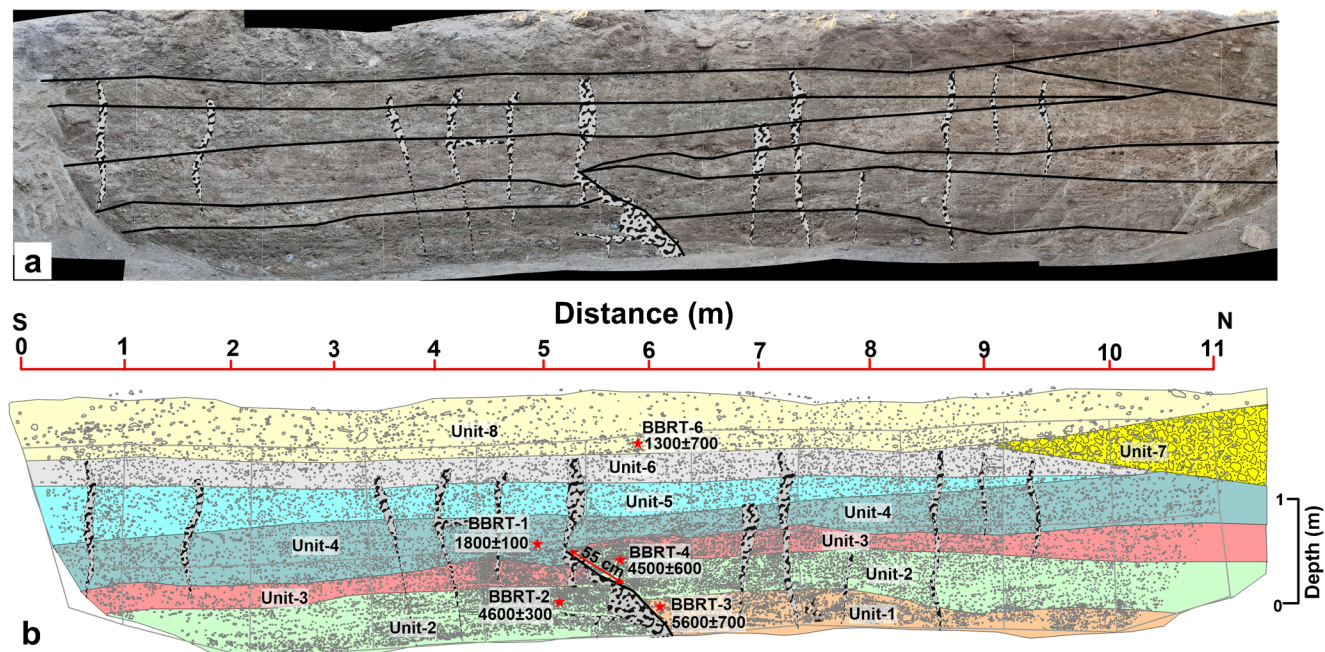


Fig. 10 (a) Photo mosaic of west wall of the trench excavated across KMF-2. Grids of 1 m × 1 m on a trench wall are marked by thin lines; (b) log of the west wall of the trench. Eight lithological units were exposed. The oldest inferred earthquake, event I, displaced the stratigraphic units 1, 2, and 3 along fault strand F1. Event II was inferred based on liquefaction features observed all along the trench wall. These liquefaction features were well injected through unit 1 and unit 6 Fig. 11 Calendar ages and probability distributions of stratigraphic units exposed in trenches excavated across the KMF. The ages are calculated and modeled using OxCal v.4.3.2 (Bronk Ramsey 2017 and

Bronk Ramsey and Lee 2013). Four earthquakes were identified: event I occurred between 3522 BC and 2876 BC; event II occurred between 2497 and 1435 BC. Event III occurred between BCE 1829 and BCE 399. Event IV gave a range of 1023 to 1259 AD and 02 BC to 427 AD which is correlated with the earthquake event that has occurred between AD 885 and 1035. Area with outlines indicates the probability distribution functions of calendar ages. Probability distribution function of trench 1 is highlighted by grey outlines, trench 2 is marked by green outline, and the reference probability distribution is marked by red outlines (Malik et al. 2017)

Timing of deformation and earthquake

Optical ages of the samples (BBR-2, BBR-3, BBR-5, BBR-7, BBR-8, BBR-9, BBR-10, BBR-11, BBR-13, and BBR-14) that were collected from the west wall of trench 1 are summarized in Fig. 9 and Table 2. Five samples collected from unit 2 yielded an age 8200 ± 600 years (BBR-2), 8300 ± 700 years (BBR-7), 8300 ± 800 years (BBR-11), 5500 ± 400 years (BBR-9), and 5000 ± 400 years (BBR-10) respectively. Three samples collected from unit 3 yielded an age of 3900 ± 400 years (BBR-3), 4400 ± 300 years (BBR-5), and 4300 ± 300 years (BBR-8). A sample collected from unit 4 yielded an age of 2900 ± 300 years (BBR-13). However, the sample collected from unit 6 yielded an age of 890 ± 70 years, respectively (Table 2). The chronometric data from the trench wall suggests that the first phase of aggradation within the trench (unit 2) was started ~ 8000 years before present and sedimentation continued intermittently until around 5000 years (Fig. 9). However, the second phase of deposition started around 4500 years and continued until around 3000 years (unit 3). Based on the special and stratigraphic relationship, it is clear that after deposition of 4000 year sediments (unit 3), first phase of faulting took place.

During the F1 faulting, the older (unit 2) 8300 year (6828 cal BC) sediments thrust over the 4 ka (3359–2501 cal BC) sediments along steeply (75° N) north-dipping plane. The second phase of faulting event F2 took place after deposition of unit 2 around 2900 years (2301–1498 cal BC). During the second phase of faulting, stratigraphic units 2, 3, 4, and 6 are displaced along a single event along gently north-dipping (33° N) fault F2 (Fig. 9). The faulting event F2 is capped by the 890 ± 70 year sediments. From stratigraphic and chronometric data, it is suggested that the younger event took place prior to 890 ± 70 ka (1289–1023 cal BC). Based on the net displacement along the F1 and F2 and the optical ages of displaced sediments, we have estimated slip rate of 0.18 mm/year for F1 and 0.39 mm/year for F2. However, the estimated uplift rate along F1 and F2 are 0.12 mm/year and 0.14 mm/year, respectively.

Optical ages of the samples (BBRT-1, BBRT-2, BBRT-3, BBRT-4, and BBRT-6) that were collected from the trench 2 are summarized in Fig. 10 and Table 2. A sample (BBRT-3) collected from unit 1 yielded an age of 5600 ± 700 years. Two samples collected from unit 2 gave an OSL age of 4600 ± 300 years (BBRT-2), and 4500 ± 600 years (BBRT-4) respectively. The OSL chronology of unit 4 gave an OSL age of 1800 ± 100 ka (BBRT-1); however, a sample collected from unit 8 yielded an age of 1300 ± 700 ka (Table 2). Based on the pattern of displacement and sedimentary dykes (capped by unit 6), two event horizons have been identified in the excavated section (west wall of trench 2) showing clear evidence of two earthquake events occurred between 2000 and 1000 years before. From the chronometric data and stratigraphic

horizons, it is clear that the units (1–3) were displaced along a north-dipping (33° N) reverse fault during an earthquake event I occurred around 2000 years. However, in the evidence from the displaced horizons and capping sediments of unit 4, it is clear that the faulting event took place prior to 1800 years (Fig. 10). The earthquake event II is evident from the vertical dykes (product of liquefaction) of various dimensions. The event II is dated around 1300 years before present ka. Based on the net displacement along the fault and the optical ages of displaced sediments, the slip rate estimated along the fault is of 0.30 mm/year and uplift rate along F is 0.17 mm/year.

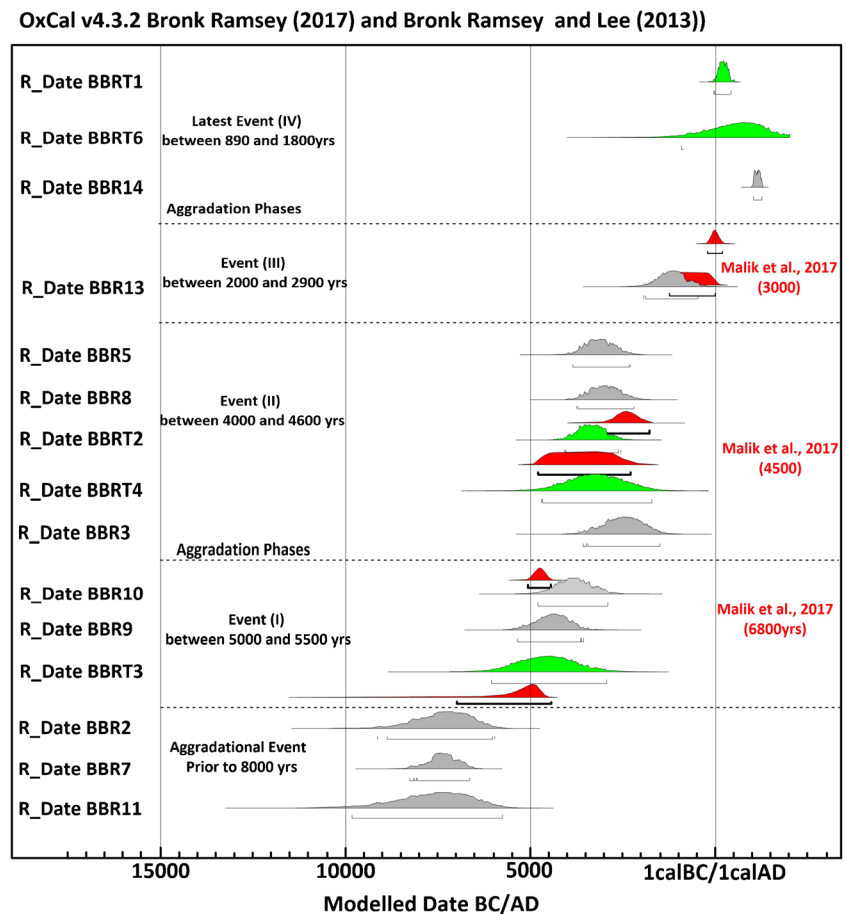
Based on modeled OSL ages and stratigraphy exposed in both the trenches, at least four earthquake events have been inferred that may occur along KMF in the last 8000 years (Figs. 9 and 10). The earthquake event I occurred between 5000 and 5500 years (3522–2876 BC) (Fig. 11); event II occurred between 4000 and 4600 years (2497–1435 BC). The events I and II were responsible for the massive damage of Harappan civilization between BCE 2900 and 1900 BCE. The event III occurred between 2000 and 2900 years, which corresponds to BCE 1829 and BCE 399, whereas the most recent event IV inferred from maximum likelihood ages obtained using the OxCal model gave a range of 1023 and 1259 AD and 02 BC to 427 AD, which is correlated with the earthquake event that has occurred between AD 885 and 1035.

Discussion and conclusion

Seismicity and crustal deformation

At present, the seismic activity in the Kachchh Rift Basin is mostly confined to the eastern portion of the Kachchh Mainland Fault (KMF) and South Wagad Fault (SWF) zones (Kothyari et al. 2016c). However, quite a few earthquakes are recorded in the Gedi Fault (GF) zone towards the northern part of Wagad, along newly activated faults that are inferred to be seismogenic (Mandal et al. 2004; Rastogi et al. 2014). The Wagad area was reactivated after the 26 January 2001 Bhuj earthquake (Mandal et al. 2004; Bodin and Horton 2004; Khan et al. 2016); since then, continuous seismicity is observed towards the eastern margin of Kachchh Basin. In the GF zone, around 50 earthquakes (M_w 3.0–4.5) have been recorded with focal depths in the range 5–20 km, during 2006–2016. A large number of aftershocks (M_w 2.2–5.7) occurred in the Wagad area between KMF and GF with focal depths ranging from 10 to 40 km. A few moderate earthquakes such as the M_w 5.0 February 2006, M_w 4.8 February 2006, M_w 5.7 March 2006, and M_w 4.1 April 2008 have occurred which are associated with the GF (Mandal et al. 2007, Kothyari et al. 2016b, 2018). This indicates that the GF is seismically still active. In the central and southern parts of

Fig. 11 Calendar ages and probability distributions of stratigraphic units exposed in trenches excavated across the KMF. The ages are calculated and modeled using OxCal v.4.3.2 (Bronk Ramsey, 2017 and Bronk Ramsey and Lee, 2013). Four earthquakes were identified: event I occurred between 3522 BC and 2876 BC; event II occurred between 2497 and 1435 BC. Event III occurred between BCE 1829 and BCE 399. Event IV gave a range of 1023 and 1259 AD and 02 BC to 427 AD, which is correlated with the earthquake event that has occurred between AD 885 and 1035. Area with outlines indicates the probability distributions functions of calendar ages. Probability distribution function of trench 1 is highlighted by gray outlines, trench 2 is marked by green outline, and the reference probability distribution is marked by red outlines (Malik et al., 2017)



the Wagad area, a few moderate earthquakes of Mw 4.5 (Sept. 2005), Mw 5.5 (2006), Mw 4.7 (May 2007), Mw 4.5 (March 2008), Mw 4.3 (Aug. 2011), and Mw 4.0 (April 2012) are found to be associated with the SWF, whereas the Mw 4.2 (May 2011), Mw 4.5 (March 2013), and Mw 5.1 (2014) earthquakes are associated with the NWF. The occurrences of these moderate earthquakes suggest that the Wagad area in eastern Kachchh is seismically active (Rastogi et al. 2014, Kothyari et al. 2016a). The GPS-driven strain distribution pattern of the Wagad area indicates an increase of compressional strain towards the western part of the Wagad upland, between KMF, SWF, and GF. Further, Kothyari et al. (2016a) inferred that the zone between KMF and SWF is accumulating higher strain (0.052μ strain/year). However, in the east of Wagad, it gradually decreases to -0.04 to -0.02μ strain/year. Accumulation of higher strain between KMF and SWF is reflected in the form of deformation of geomorphic landforms in the basin (Kothyari et al. 2016c). The GPS study reveals that Kachchh Rift Basin (KRB) is accumulating up to 3 mm/year of NE directed motion of Indian plate. Most of the GPS sites in the Kachchh region indicate maximum deformation in the range of 1 to 3 mm/year (Dumka and Rastogi 2013).

Active faulting and neotectonic deformation

Previous paleoseismic investigations have been limited to a few faults in the Kachchh region of Western Peninsular India (Mc-Calpin and Thakkar, 2006; Malik et al. 2008; Morino et al. 2008; Kundu et al. 2010; Kothyari et al. 2016a and b). In the present study, we have presented the results of paleoseismic investigations in the central part of the KMF. We combine the observations of north-dipping KMF presented here with the recently published results (Mohan et al. 2018; Kothyari et al. 2016a, b). The trench investigation by Malik et al. (2008) near Lodai area, which is located ~ 40 km east of the present location, reveals the displacement (98 cm) of Late Pleistocene to Holocene alluvial fan surfaces along a high-angle (55°) reverse fault dipping towards the south. However, the paleoseismic investigation by Morino et al. (2008) near Jhura ~ 10 km east of present location revealed displacement (5 m) of overbank deposits along a low-angle (15°) reverse fault dipping towards the south. The trenches of Malik et al. (2008) at Lodai and Morino et al. (2008) at Jhura are located close to transverse faults showing south dip of KMF. Globally, it is well proven that the transverse faults

are responsible for the change in the dip direction as in the San Andreas Fault system in Southern California (Nicholson et al. 1986), the Lake Mead Fault system in the Basin and Range province (Ron et al. 1986), and the Alpine Fault system in New Zealand (Lamb 1989). However, the present study shows that the fault is north-dipping fault. The KMF is dissected by several NE-SW and NW-SE oriented transverse faults. These transverse faults have segmented the KMF into several fault-bound segments (Kothyari et al. 2019). Change in dip directions of the KMF is possible because of differential motion along each segment. The observation of north-dipping KMF and relation with transverse fault are well discussed by Mohan et al. (2018). Based on the optical chronology of the strath terraces, Mathew et al. (2006) and Prizomwala et al. (2016) provided the uplift rate 1 ± 0.05 mm/year for the eastern segment of the KMF. Further, Kothyari et al. (2016a) reported that the SWF breaks the late Holocene 3 ka sediments within the epicenter zone of 26 January 2001 Bhuj event. It is also noticed that the 3 ka uplift event is responsible for the evolution of the present-day fluvial landforms along the SWF zone. Further, Kothyari et al. (2016a) opine that the SWF zone is uplifting at the rate of ~ 2.8 mm/year. However, based on displaced sedimentary units and uplift of Holocene terrace surfaces, Kothyari et al. (2016b) provided long-term uplift rate 0.3–1.1 mm/year along the GF. It has been observed that several domes and anticlines are developed parallel to the KMF zone. The most recent study advocates that these anticlines are developed as a result of fault-related growth, into segments with lateral propagation, leading to a single large segment through linkage of smaller segments (Mathew et al. 2006). However, the presence of domes and anticlines between Nirona and Bihar area is a result of compressive forces generated by different wedge bounded block faulting. The development of canyon, incision by the river, knickpoints, ponding of river, and unpaired strath terraces are remarkable geomorphic expressions identified between Nirona and Bihar area confirming active nature of the KMF (Kothyari et al. 2019). In the present study, we used strath terraces to estimate the timing of aggradation and incision. Based on the optical ages of strath terraces, we have estimated the long-term uplift rate as 0.37 to 1.48 mm/year for the hanging wall block of the KMF zone.

Active fault geometry and wide range deformation

The displacements during paleo-earthquakes and event chronology suggest that total two earthquake events (I–II) have occurred along F1 and F2 fault strands in trench 1 (Fig. 9). However, trench 2 shows displacement along a single event (fault event III), whereas the younger event has occurred in the form of paleo-liquefaction (event IV; Fig. 10). The paleo-earthquakes have folded and faulted the lithounits (2–5)

during F2 (event II), while the units 2 and 3 were displaced during the event I along F1. The unit 4 was displaced twice along F1 and F2 during events I and II. The unit 2 exhibits a net displacement of 80 cm along F1 and cumulative displacement of 115 cm along F2 (Fig. 9). Units 4 and 5 were displaced once with a slip of about 25 cm along with F2 during event II. This suggests that a total displacement of 140 cm has occurred during the initial part of Late Holocene earthquake event II, along F2 (Fig. 9). The section of trench 2 exhibits movement during the paleo-earthquake that has faulted lithounits 1 to 3 along a single fault (event III; Fig. 10). The unit 2 exhibits a net displacement of 55 cm along F1. The evidence of the second event is observed all along the trench wall that reflects in the form of paleo-liquefaction. These liquefaction features are injected through the unit 1 to unit 6 and might have occurred during a Late Holocene earthquake (event IV; Fig. 10). For calculating the geometric parameters from both the trenches, we have considered the slip, folded-displaced lithounits along F1 and F2 fault strands. We have used the cumulative slip (80 cm and 115 cm) of unit 2 within the trench 1 and 55 cm of unit 2 from trench 2 to calculate the geometric parameters. Considering the fault angle $\theta = 75^\circ$, the slip of 80 cm and vertical separation of 50 cm were obtained along F1. However, the angle along F2 is $\theta = 33^\circ$, the slip is 115 cm, and the vertical separation of 40 cm is measured from the trench 1, whereas the fault angle $\theta = 33^\circ$, slip 55 cm, and vertical separation 30 cm is measured along the fault from trench 2. We have used optical ages of sedimentary units to estimate slip rate and uplift rates of displaced horizons for both the trenches. The estimated slip rate along F1 is 0.18 mm/year and the uplift rate is 0.12 mm/year; however, for F2, the observed slip rate is 0.39 mm/year and the uplift rate is 0.14 mm/year, whereas the faulting event from trench 2 shows slip rate 0.30 mm/year and the uplift rate 0.17 mm/year respectively. The observed slip difference between F1 and F2 of trench 1 is 0.21 mm/year. However, about 32% slip is accommodated by F1 and about 68% slip is accommodated by F2. The wide zone of deformation from trench 1 and trench 2 suggests that 65% of the slip is accommodated by NF-1 and about 35% of the slip is consumed by NF-2.

The identification of paleo-earthquake and understanding the pattern of their occurrence is extremely important to assess the seismic hazard in Western Peninsular India. Several moderate to large magnitude earthquakes (Mw 6 to Mw 7.8) have occurred in the Kachchh region of Western India during the historic past (Bilham 1998; Bisht 1994; Rajendran 2000; Rajendran and Rajendran 2001, Rajendran et al. 2003; Rajendran et al. 2008). Our trench investigation along the KMF between Nirona and Bihar villages revealed the occurrence of at least four paleo-earthquakes, i.e., event I occurred between 5000 and years, event II occurred between 4000 and 4600 years, event III occurred between 2000 and years, and event IV occurred between 1023 and 1259 AD and 02 BC to

427 AD. It is very difficult to correlate these events with the historical earthquake, because of non-availability of earthquake information during Middle to Late Holocene from the Kachchh region of Western India. However, few studies pertaining to Middle and Late Holocene earthquakes have been provided by Rajendran and Rajendran (2001 and 2003) based on morphological changes and liquefaction features. Trench investigation and liquefaction studies by Rajendran (2000) suggest that there was an earthquake in the Kachchh region between cal AD 885–1035. Our trench site is located approximately 85 km southeast of trench site of Rajendran (2000) (Fig. 1b). The west wall of trench shows displacement of stratigraphic units 2, 3, 4, and 5 along a north-dipping fault (Fig. 9). The faulting event was capped by 890 year sediments, which is correlated with the earthquake event that has occurred between AD 885 and 1035. The historic records show that the western part of India was inhabited 4000–5000 years ago (Dales 1966; Bisht 1994; Rajendran and Rajendran 2001). Historical accounts indicate that in the western part of India, an earthquake has occurred between AD 712 and 1361 (e.g., Williams 1958), which probably may have occurred on the northern shores of the Rann of Kachchh (Rajendran and Rajendran 2001). Our trench site is located approximately 200 km southeast of 1361 AD event (Fig. 1b). The liquefaction features observed in the present study and chronometric data also suggests that there was an earthquake ~ 1300 years (Fig. 10), which we are trying to correlate with the 1361 AD earthquake. Evidence from the disposition of human skeletons and the well-built brick structures indicates that another earthquake has occurred about 700–800 years ago. However, the landscape changes such as tilting and migration of Indus River towards the west and uplift of Rann of Kachchh further indicate an earthquake activity around 997–1030 AD (Williams 1958; Wilhelmy 1969). Besides these changes, evidence from the uplift of Nara River channel and destruction of settlement along its bank indicates that the Rann of Kachchh was uplifted by 4–6 m during an earthquake (Oldham 1926). Further, studies based on the geomorphic investigation of incised channels close to the epicenter of 1819 earthquake suggest that there was an earthquake around 2 ka (Tyagi et al. 2012). The information we have generated will be helpful in understanding the frontal fault dynamics towards better seismic hazard evaluation in the Kachchh region of Western India.

Conclusions

In the study based on the detailed paleoseismic trench investigation, optical chronology allows us to draw the following conclusions.

1. The trench log geometry combined with optical chronology shows four earthquake events that have occurred during the last 5600 to 1000 years.
2. Paleoseismic investigation along trench 1 along KMF-1 suggests the occurrence of at least two large magnitude earthquakes along F1 and F2. The timing of earthquake along F1 is postdated to 4000 years; however, the timing of earthquake along F2 is bracketed between 890 and 2000 ka. It is correlated with the earthquake occurred between AD 885 and 1035.
3. Paleoseismic investigation along trench 2 along KMF-2 suggests occurrence of at least two large magnitude earthquakes between the period 4500 and 1300 years. The timing of earthquake event I is predated to 1800 years and occurred between the 4500 and 1800 ka.
4. The second large event II is inferred based on liquefaction features observed along the trench wall. The event is predated to 1300 years. It is correlated with the Indus Delta earthquake occurred between 712 and 1361 AD.
5. The chronometric data of uplifted fluvial strath terrace deposits, developed along the hanging wall block of KMF, shows the vertical uplift rate of 0.37–1.48 mm/year.
6. Based on displaced stratigraphic units and optical ages, the estimated average slip rate is 0.28 mm/year and the uplift rate is 0.13 mm/year along KMF-1, over an interval of 1800–4000 years. However, the estimated slip rate along KMF-2 is of the order of 0.30 mm/year and the observed uplift rate is 0.17 mm/year.
7. The paleoseismic investigation, fault length, width, and chronometric data suggested that the area is undergoing a quiescent period of ~ 1000 years in terms of generation of moderate to large earthquake.
8. Based on detailed paleoseismic trench investigations and optical chronology, the following conclusions can be drawn from this study.

Acknowledgments GCK is thankful to Dr. Sumer Chopra, Director, Institute of Seismological Research, for critical review of the manuscript. We are thankful to Dr. M. Ravikumar, Director General, Institute of Seismological Research, for his encouragement throughout the work. The authors are thankful to Dr. Cengiz Zabcı for his constructive comments for improving the manuscript.

Funding information The authors are grateful to the Ministry of Earth Sciences, Government of India (MoES/P.O.(Seismo)/1(270)/AFM/2015) for the financial support under the active fault mapping program.

References

- Adams J, Halchuk S (2003) Fourth generation seismic hazard maps of Canada: values for over 500 Canadian localities intended for the 2005 National Building Code of Canada: Geological Survey of Canada Open File 4459, 155 p

- Adams J, Basham PW, Halchuk S (1995) Northeastern North America earthquake potential—new challenges for seismic hazard mapping, in *Current Research, 1995-D: Ottawa, Ontario, Geological Survey of Canada*, pp 91–99
- Arnold LJ, Roberts RG, Galbraith RF, Delong SB (2009) A revised burial dose estimation procedure for optical dating of young and modern age sediments. *Quat Geochronol* 4:306–325
- Audemard FA (1999) Morpho-structural expression of active thrust fault systems in the humid tropical foothills of Colombia and Venezuela. In: Frisch W (ed) *Proc. Fourth Int. Conf. Geomorphology, Bologna 1997. Z. Geomorph., N.F., v 118*, pp 1–18
- Bailey RM, Arnold LJ (2006) Statistical modelling of single grain quartz distributions and an assessment of procedures for estimating burial dose. *Quat Sci Rev* 25:2475–2502
- Baker WE (1846) Remarks on the Allah Bund and on the drainage of the eastern part of the Sind basin. *Transactions Bombay Geographic Society* 7:186–188
- Beck RA, Burbank DW, Sercombe WJ, Riley GW, Bamdr JK, Berry JR, J Afzal, Khan AM, Jurgen H, Metje J, Cheema A, Shafique NA, Lawrence RD, Khan MA (1995) Stratigraphic evidences for an early collision between India and Asia. *Nature* 373:55–58
- Besse J, Courtillot V, Pozzi PJ, Westphal M, Zhou YX (1984) Paleomagnetic estimates of crustal shortening in the Himalayan thrusts and zangbo suture. *Nature* 331:621–626
- Bilham R (1998) Slip parameters for the Rann of Kachchh, India, 16 July 1819, earthquake quantified from contemporary accounts. In: Stewart IS, Vita Finzi C (eds) *Coastal tectonics. Geological Society of London Spec Publ* 146:295–319
- Bisht RS (1994) Secrets of the water fort. *Down to Earth* 2:25–31
- Bisht RS (2011) Major earthquake occurrences in archaeological strata of Harappan settlement at Dholavira (Kachchh, Gujarat). *International symposium on the 2001 Bhuj earthquake and advances in earthquake science, AES 2011, ISR, Gandhinagar, Gujarat, S16_IGCP-11*, pp 112–113
- Biswas SK (1977) Mesozoic rock stratigraphy of Kutch. *Q J Geol Min Metall Soc India* 49:1–52
- Biswas SK (1982) Rift Basin in Western margin of India and their hydrocarbon prospects with special reference to Kachchh Basin. *Am Assoc Petroleum Geol Bull* 66:1497–1513
- Biswas SK (1987) Regional tectonic framework, structure and evolution of the western marginal basin of India. *Tectonophysics* 135:307–327
- Biswas SK (1993) Tectonic framework and evolution of graben basins of India. *Indian Jour Petro Geol* 1(2):276–292
- Biswas SK (2005) A review of structure and tectonics of Kachchh Basin, Western India with special reference to Earthquakes. *Curr Sci* 88(10):1592–1600
- Biswas SK (2016) Tectonic framework, structure and tectonic evolution of Kutch Basin, Western India, Special Publication of the Geological Society of India, No. 6, pp 129–150
- Biswas SK, Khattri KN (2002) A geological study of earthquakes in Kachchh, Gujarat, India. *J Geol Soc India* 60:131–142
- Bodin P, Horton S (2004) Source parameters and tectonic implications of aftershocks of the Mw7.6 Bhuj earthquake of 26 January 2001. *Bull Seismol Soc Am* 94(3):818–827
- Boetter-Jensen L, Duller GAT, Murray AS (2003) Advances in luminescence measurement systems. *Radiat Meas* 32:523–528
- Bronk Ramsey C (2017) Methods for summarizing radiocarbon datasets. *Radiocarbon* 59(2):1809–1833
- Bronk Ramsey C, Lee S (2013) Recent and planned developments of the program OxCal. *Radiocarbon* 55(2-3):720–730
- Bull WB (1991) *Geomorphic response to climate changes*. Oxford University Press, Oxford, 326 p
- Bull WB, McFadden LD (1977) Tectonic geomorphology north and south of the Garlock Fault, California. In: Doehering DO (ed) *Geomorphology in arid regions: Proceedings at the Eighth Annual Geomorphology Symposium*. State University of New York, Binghamton, NY, pp 115–138
- Burnes A (1835) Memoir on the eastern Branch of the River Indus, giving an account of the alterations produced on it by an earthquake, also a theory of the formation of the Runn and some conjectures on the route of Alexander the Great; drawn up in the years 1827–1828. *R Asiatic Soc Trans* 3:550–588
- Burbank D, Anderson R, (2001) *Tectonic geomorphology*. Blackwell Science. (274 pp.)
- Chandrasekhar DV, Mishra DC (2002) Some geodynamic aspects of Kachchh basin and seismicity: an insight from gravity studies. *Curr Sci* 83:492–498
- Chandrasekhar E, Mathew G, Harinarayana T (2012) A new hypothesis for the deep subsurface structures near the Bhuj 2001 earthquake (Mw 7.6) hypocenter zone and its tectonic implications. *Geophys J Int* 190:761–768
- Chowksey V, Maurya DM, Joshi P, Khonde N, Das A, Chamyal LS (2011) Lithostratigraphic development and neotectonic significance of the Quaternary sediments along the Kachchh Mainland Fault (KMF) zone, Western India. *J Earth Syst Sci* 120(6):979–999
- Christie-Blick N, Biddle K (1985) Deformation and basin formation along strike-slip fault. *SEPM Spec Publ* 37. <https://doi.org/10.2110/pec.85.37.0001>
- Ron H, Aydin A, Nur A (1986) Strike-slip faulting and block rotation in the Lake Mead fault system. *Geology* 14:1020–1023
- Chung WP, Gao H (1995) Source parameters of the Anjar earthquake of July 21, 1956, India, and its seismotectonic implications for the Kachchh Rift Basin. *Tectonophysics* 242:281–292
- Costain JK, Bollinger GA, Speer JA (1987) Hydroseismicity: a hypothesis for the role of water in the generation of intraplate seismicity. *Seismol Res Lett* 58:41–64
- Courtillot V, Besse J, Vandamme D, Montigny R, Jaeger JJ, Cappetta H (1986) Deccan flood basalts at the Cretaceous/Tertiary boundary. *Earth Planet Sci Lett* 80:361–374
- Cowie PA (1998) A healing–reloading feedback control on the growth rate of seismogenic faults. *J Struct Geol* 20:1075–1087
- Dahlstrom CDA (1970) Structural geology in the eastern margin of the Canadian Rocky Mountains. *Bull Can Petrol Geol* 18:332–406
- Dales GF (1966) The decline of the Harappans. *Scientific Am* 214:92–100
- Dewey J, Cande S, Pitman W (1989) The tectonic evolution of the India/Eurasia collision zone. *Eclogae Geologicae Helvetiae* 82:717–734
- Dumka, R.K., and Rastogi, B.K. (2013). Crustal strain in the rupture zone of 2001 Bhuj earthquake, Annual Report 2012–2013, Institute of Seismological Research, p.45–46
- Durcan JA, King GE, Duller GAT (2015) DRAC: Dose Rate and Age Calculator for trapped charge dating. *Quaternary Geochronology* 28:54–61
- Flint JJ (1974) Stream gradient as a function of order, magnitude, and discharge. *Water Resour Res* 10:969–973
- Frere HBE (1870) Notes on the Runn of Cutch and neighboring region. *J R Geogr Soc Lond* 40:181–207
- Ghosh SK (1993) *Structural geology: fundamentals and modern developments*, 1st edn. Elsevier Publications, pp 376
- Glennie KW, Evans G (1976) A reconnaissance of the recent sediments of Rann of Kachchh, India. *Sedimentology* 23:625–647
- Goldrick G, Bishop P (2007) Regional analysis of bedrock stream long profiles: evaluation of Hack's SL form, and formulation and assessment of an alternative (the DS form). *Earth Surf Process Landf* 32(5):649–671
- Gombos AM Jr, Powell WG, Norton IO (1995) The tectonic evolution of Western India and its impact on hydrocarbon occurrences: an overview. *Sedimentary Geology* 96:119–129
- Gowd TN, Rao SVS, Gaur VK (1992) Tectonics stress field in the India Subcontinent. *J Geophys Res* 97:11879–11888

- Gupta S, Cowie PA, Dawers NH, Underhill JR (1998) A mechanism to explain rift-basin subsidence and stratigraphic patterns through fault array evolution. *Geology* 26:595–598
- Hack J (1973) Drainage adjustment in the Appalachians. In: Morisawa M (ed) *Fluvial geomorphology*. George Allen and Unwin, London, pp 51–69
- Harbor D, Gunnell Y (2007) Along-strike escarpment heterogeneity of the Western Ghats: a synthesis of drainage and topography using digital morphometric tools. *J Geol Soc India* 70:411–426
- Jacob LG (1860) Extracts from a journal I kept during a tour made in 1851 through Kachchh. *Trans Bombay Geograph Soc* 15:56–66
- Jaeger JJ, Courtillot V, Tapponnier P (1989) Paleontological view of the ages of the Deccan Traps, the Cretaceous/Tertiary boundary, and the Indian-Asian collision. *Geology* 17:316–319
- Johnston AC (1996) Seismic moment assessment of earthquakes in stable continental regions. II. Historical seismicity. *Geophys J Int* 125: 639–678
- Johnston AC, Kanter LR (1990) Earthquakes in stable continental crust. *Sci Am* 262:68–75
- Joshi PN, Maurya DM, Chamyal LS (2012, 2013) Geomorphology morphotectonic segmentation and spatial variability of neotectonic activity along the Narmada–Son Fault, Western India: remote sensing and GIS analysis. *Geomorphology*:180–181–292–306. <https://doi.org/10.1016/j.geomorph.2012.10.023>
- Kale VS, Shejwalkar N (2008) Uplift along the western margin of the Deccan Basalt Province: is there any geomorphometric evidence? *Jour Earth Sys Sci* 117:959–971
- Khan PK, Mohanty S p, Sinha S, Singh D (2016) Occurrences of large-magnitude earthquakes in the Kachchh region, Gujarat, Western India: tectonic implications. *Tectonophysics* 679:102–116
- Kingma JT (1958) Possible origin of piercement structures, local unconformities and secondary basins in the Eastern Geosyncline, New Zealand. *N.Z. Geol Geophys* 1:269–274
- Kothiyari GC, Rastogi BK, Dumka RK, Chauhan M (2015) Secondary surface deformation along the Bharudia/ North Wagad Fault Zone in Kachchh Rift Basin, Western India. *Comunicações Geológicas* 102(1):15–27
- Kothiyari GC, Rastogi BK, Morthekai P, Dumka RK, Kandregula RS (2016a) Active segmentation assessment of the tectonically active South Wagad Fault in Kachchh, Western Peninsular India. *Geomorphology* 253:491–507
- Kothiyari GC, Rastogi BK, Morthekai P, Dumka RK (2016b) Landform development in a zone of Active Gedi Fault, Eastern Kachchh Rift Basin, Western India. *Tectonophysics* 670:115–126
- Kothiyari GC, Dumka RK, Singh AP, Chauhan G, Thakkar MG, Biswas SK (2016c) Tectonic evolution and stress pattern of South Wagad Fault at the Kachchh Rift Basin in Western India. *Geol Mag*. <https://doi.org/10.1017/S0016756816000509>
- Kothiyari, G. C, Singh, A. P., Mishra S., Kandregula, R. S., Chaudhary I., Chauhan G. (2018). Evolution of drainage in response to brittle-ductile dynamics and surface processes in Kachchh Rift Basin Western India. *Tectonics-A Problem of Regional settings*. Intech Open. <https://doi.org/10.5772/intechopen.73653>
- Kothiyari CC, Shirvalkar P, Kandregula RS, Rawat YS, Dumka RK, Joshi N (2019) Holocene tectonic activity along Kachchh Mainland Fault: impact on late mature Harappan civilization, Kachchh, Western India. *Quaternary International* (in press)
- Keller EA, Pinter N (1996) *Active tectonics: earthquakes, uplift, and landscape*, 1st edn. Prentice hall, New Jersey, p 338
- Kundu HS, Thakkar MG, Biswas RH, Singhvi AK (2010) Optical dating of sediments in Khari River Basin and slip rate along Katrol Hill Fault (KHF), Kachchh India. *Geochronometria* 37:21–28
- Lamb S (1989) Rotations about vertical axes in part of the New Zealand plate-boundary zone, theory and observation. In: Kissel C, Laj C (eds) *Paleomagnetic rotations and continental deformation*. NATO ASI Series C Vol. 254. Kluwer, Dordrecht, Netherlands, pp 473–488
- Larson KM, Bürgmann R, Bilham R, Freymueller JT (1999) Kinematics of the India-Eurasia collision zone from GPS measurements. *J Geophys Res* 104(B1):1077–1093
- Lensen GJ (1958) A method of graben and horst formation. *J Geol* 66: 579–587
- Liu L, Zoback MD (1997) Lithospheric strength and intraplate seismicity in the New Madrid seismic zone. *Tectonics* 16:585–595
- Mac Murdo J (1824) Papers relating to the earthquake which occurred in India in 1819. *Philos Mag* 63:105–177
- Malik JN, Sohoni PS, Karanth RV, Merh SS (1999) Modern and historic seismicity of Kachchh Peninsular, Western India. *J Geol Soc India* 54:545–550
- Malik JN, Sohoni PS, Merh SS, Karanth RV (2001) Active tectonic control on alluvial fan architecture along the Kachchh Mainland Hill Range, Western India. *Zeitschrift Fur Geomorphologie* 45: 81–100
- Malik JN, Morino M, Mishra P, Bhuiyan C, Kaneko F (2008) First active fault exposure identified along Kachchh Mainland Fault: evidence from trench excavation near Lodai village, Gujarat, Western India. *J Geol Soc India* 71:201–208
- Malik JN, Gadhavi MS, Kothiyari GC, Satuluri S (2017) Paleo-earthquake signatures from the South Wagad Fault (SWF), Wagad Island, Kachchh, Gujarat, Western India: a potential seismic hazard. *J Struct Geol* 95:142–159
- Mandal P, Chadha RK, Raju IP, Kumar N, Satyamurty C, Narsaiah R (2007) Are The 7th March 2006 Mw 5.6 event and the 3rd February 2006 Mw 4–5.8 event triggered by the five years continued occurrence of aftershocks of the 2001 Mw 7.7 Bhuj Event. *Current Science* 92:1114–1124
- Mandal P, Rastogi BK, Satyanarayana HVS, Kousalya M, Vijayraghavan R, Satyamurty C, Raju IP, Sarma ANS, Kumar N (2004) Characterization of the causative fault system for the 2001 Bhuj earthquake of Mw 7.7. *Tectonophysics* 378:105–121
- Mandal P (2016) Variations of seismic velocities in the Kachchh rift zone, Gujarat, India, during 2001–2013. *Tectonophysics* 672–673:68–86
- Mathew G, Singhvi AK, Karanth RV (2006) Luminescence chronometry and geomorphic evidence of active fold growth along the Kachchh Mainland Fault (KMF), Kachchh, India: seismotectonic implications. *Tectonophysics* 422:71–87
- Maurya DM, Thakkar MG, Chamyal LS (2003) Implications of transverse fault system on tectonic evolution of Mainland Kachchh, Western India. *Curr Sci* 85:661–667
- Maurya DM, Chowksey V, Patidar AK, Chamyal LS (2016) A review and new data on neotectonic evolution of active faults in the Kachchh Basin, Western India: legacy of post-Deccan Trap tectonic inversion. In: Mukherjee, S., Misra, A.A., Calve's, G., Neme'ok, M. (Eds.), *Tectonics of the Deccan large igneous province*. Geological Society, London, Special Publications Vol. 445 (First published online September 19, 2016). <https://doi.org/10.1144/SP445.7>
- Massotti S (2007) Geodynamic models for earthquake studies in intraplate North America. *Geol Soc Am Spec Pub* 425:17–35
- McCalpin JP (1996) *Paleoseismology*. Academic Press, London, pp 583
- Mccalpin J, Carver G (2009) Chapter 5 Paleoseismology of compressional tectonic environments. *Int Geophys* 95:315–419. [https://doi.org/10.1016/S0074-6142\(09\)95005-7](https://doi.org/10.1016/S0074-6142(09)95005-7)
- Mc-Calpin J, Thakkar MG (2003) 2001 Bhuj-Kachchh earthquake: surface faulting and its relation with neotectonics and regional structures, Gujarat, Western India. *Ann Geophys* 46(5):937–956
- Merritts DJ, Vincent KR, Wohl EE (1994) Long river profiles, tectonism, and eustasy: a guide to interpreting fluvial terraces. *J Geophys Res* 99:14031–14050
- Michetti AM, Hancock PL (1997) Paleoseismology: understanding past earthquakes using quaternary geology. *J Geodyn* 24(1–4):3–10

- Michetti AM, Franck A, Audemard M, Marco S (2005) Future trends in paleoseismology: integrated study of the seismic landscape as a vital tool in seismic hazard analyses. *Tectonophysics* 408(2005):3–21
- Morino M, Malik JN, Gadhavi MS, Ansari K, Bhuiyan C, Mishra P, Kaneko F (2008) Active low-angle reverse fault and wide quaternary deformation identified in Jhura Trench across the Kachchh Mainland Fault Kachchh, Gujarat, India. *J Geol Soc Japan* 29:71–77
- Mohan K, Sastry RS, Harinarayana T, Rastogi BK (2010) New findings in the epi-center zone of 2001, Kachchh earthquake using magnetotelluric studies. In: As abstract in the proceedings of 7th Annual Meeting of Asia Oceania Geoscience Society (AOGS) during 5th to 9th July 2010 at Hyderabad International Convention Centre, Hyderabad, Session SE03 Paper A002
- Mohan K, Rastogi BK, Chaudhary P (2015) Magnetotelluric studies in the epicenter zone of 2001, Bhuj earthquake. *J Asian Earth Sci* 98: 75–84
- Mohan K, Chaudhary P, Patel P, Chaudhary BS, Chopra S (2018) Magnetotelluric study to characterize Kachchh Mainland Fault (KMF) and Katrol Hill Fault (KHF) in the western part of Kachchh region of Gujarat, India. *Tectonophysics* 726:43–61. <https://doi.org/10.1016/j.tecto.2018.01.018>
- Pavan Kumar G, Chaudhary I, Nagar M, Chouhan AK, Prizomwala SP, Mahesh P, Chopra S (2018) Transient electromagnetic investigations in a tectonic domain of the Kachchh intraplate region, Western India: a morphotectonic study of the Kachchh Mainland Fault. *Tectonics* 37:4239–4260. <https://doi.org/10.1029/2017TC004884>
- Murray AS, Wintle AG (2000) Luminescence dating of quartz using an improved single aliquot regenerative-dose protocol. *Radiat Meas* 32:57–73
- Naganjaneyulu K, Ledo JJ, Queralt P (2010) Deep crustal electromagnetic structure of Bhuj earthquake region (India) and its implications. *Geol Acta* 18:83–97
- Nelson RE (1846) Notice of an earthquake and a probable subsidence of the land in the district of Kachchh, near the mouth of the Koree, or eastern branch of the Indus, in June 1845. *Quart J Geol Soc London* 2:103
- Nicholson C, Seeber L, Williams P, Sykes L (1986) Seismic evidence for conjugate slip and block rotation within the San Andreas fault system, Southern California. *Tectonics* 5:629–648
- Oldham RD (1926) The Cutch (Kachchh) earthquake of the 16th June, 1819 with a revision of the great earthquake of the 12th June, 1897. *India Geol Survey Memoir* 46:71–147
- Oldham T (1883) A catalogue of Indian earthquakes from the earliest time to the end of AD 1869. *Mem Geol Surv India* 19:163–213
- Patidar AK, Maurya DM, Thakkar MG, Chamyal LS (2007) Fluvial Geomorphology and Neotectonic activity based on field and GPR data, Katrol Hill Range, Kachchh, Western India. *Quat Int* 159:74–92
- Patidar AK, Maurya DM, Thakkar MG, Chamyal LS (2008) Evidence of neotectonic reactivation of the Katrol Hill Fault during Late Quaternary and its GPR characterization. *Curr Sci* 94:338–346
- Patriat P, Achache J (1984) India-Eurasia chronology and its implications for crustal shortening and deriving mechanisms of plates. *Nature* 311:615–621
- Pazzaglia FJ (2013) Fluvial terraces treatise on geomorphology. 9. <https://doi.org/10.1016/B978-0-12-374739-6.00248-7>
- Pollitz FF, Kellog L, Burgmann R (2001) Sinking mafic body in a reactivated lower crust: a mechanism for stress concentration at the New Madrid seismic zone. *Bull Seismol Soc Am* 91:1882–1897
- Prescott JR, Stephan LG (1982) Contribution of cosmic radiation to environmental dose. *Pact* 6:17–25
- Prizomwala SP, Das A, Chauhan G, Solanki T, Basavaiah N, Bhatt N, Thakkar MG, Rastogi BK (2016) Late Pleistocene-Holocene uplift driven terrace formation and climatetectonic interplay from a seismically active intraplate setting: an example from Kachchh, Western India. *J Asia Earth Sci* 124:55–67
- Quittmeyer RC, Jacob KH (1979) Historical and modern seismicity of Pakistan, Afghanistan, northern and southern Iran. *Bull Seismol Soc Am* 69:773–823
- Rajendran, C. P., (2000) Using geological methods for earthquake studies: a perspective from peninsular India, *Seismology 2000, Current Science: Special Section*, K. Rajendran and C. P. Rajendran (Editors), Indian Acad. Sci., Bangalore, India, 79, 1251–1258
- Rajendran CP, Rajendran K (2001) Characteristics of deformation and past seismicity associated with the 1819 Kachchh earthquake, Northwestern India. *Bull Seismol Soc Am* 91(3):407–426
- Rajendran K, Rajendran CP (1999) Seismogenesis in the stable continental interiors: an appraisal based on two examples from India. *Tectonophysics* 305:355–370
- Rajendran CP, Rajendran K, John B (1998) Surface deformation related to the 1819 Kachchh earthquake: evidence for recurrent activity. *Curr Sci* 75(6):623–626
- Rajendran K, Rajendran CP, Thakkar MG, Tuttle MP (2001) Kachchh (Bhuj) Earthquake: coseismic surface features and their significance. *Curr Sci* 80(11):1397–1405
- Rajendran CP, Rajendran K, Vora KH, Gaur AS (2003) The odds of a seismic source near Dwarka, NW Gujarat: an evaluation based on proxies. *Curr Sci* 84:695–701
- Rajendran CP, Rajendran KM, Thakkar MG, Bhanu G (2008) Assessing the previous activity at the source zone of the 2001 Bhuj earthquake based on the near-source and distant paleoseismological indicators. *J Geophys Res* 113:B05311. <https://doi.org/10.1029/2006jb004845>
- Rastogi BK, Mandal P, Biswas SK (2014) Seismogenesis of earthquakes occurring in the ancient Rift Basin of Kachchh, Western India. In: Talwani P (ed) *Intraplate earthquakes*, pp 126–161
- Roberts GP, Michetti AM (2004) Spatial and temporal variations in growth rates along active normal fault systems: an example from the Lazio–Abruzzo Apennines, Central Italy. *J Struct Geol* 26:339–376
- Sarkar D, Sain K, Reddy PR, Catchings RD, Mooney WD (2007) Seismic reflection images of the crust beneath the 2001 M=7.7 Kutch (Bhuj) epicentral region, Western India. *Geol Soc Am Spec Pap* 425:319–327
- Sastry RS, Nagarajan N, Sarma SVS (2008) Electrical imaging of deep crustal features of Kutch, India. *Geophys J Int* 172(3):934–944. <https://doi.org/10.1111/j.1365-246X.2007.03658.x>
- Seeber L, Gornitz V (1983) River profiles along the Himalayan arc as indicators of active tectonics. *Tectonophysics* 92(4):335–367. [https://doi.org/10.1016/0040-1951\(83\)90201-9](https://doi.org/10.1016/0040-1951(83)90201-9)
- Serva L, Blumetti AM, Guerrieri L, Michetti AM (2002) The Apennine intermountain basins: the result of repeated strong earthquakes over a geological time interval. *Boll Soc Geol Ital Speciale* 1(2001):939–946
- Sohoni PS, Malik JN (1998) Remnants of large magnitude earthquakes: evidences from the great rann sediments Kachchh, Western India. *Curr Sci* 74:985–989
- Sohoni PS, Malik JN, Merh SS, Karanth RV (1999) Active tectonics astride Katrol Hill Zone, Kachchh W. India. *J Geol Soc India* 53: 579–586
- Siveright R (1907) Cutch and the Ran. *Geogr J* XXIX:519–539
- Snyder NP, Whipple KX, Tucker GE, Merritts DJ (2000) Landscape response to tectonic forcing: digital elevation model analysis of stream profiles in the Mendocino triple junction region, Northern California. *Geol Soc Am Bull* 112:1250–1263. <https://doi.org/10.1130/0016-7606>
- Talwani P, Acree SD (1984) Pore pressure diffusion and the mechanism of reservoir induced seismicity: pure and applied geophysics, v. 122, pp 947–965
- Talwani P, Gangopadhyay A (2001) Tectonic framework of the Kachchh earthquake of 26 January 2001. *Seismol Res Lett* 72:336–345

- Thakkar MG, Ngangom M, Thakkar PS, Juyal N (2012) Terrain response to the 1819 Allah Bund earthquake in western Great Rann of Kachchh Gujarat, India. *Curr Sci* 103:108–112
- Tyagi AK, Shukla AD, Bhushan R, Thakkar PS, Thakkar MG, Juyal N (2012) Mid-Holocene sedimentation and landscape evolution in the western Great Rann of Kachchh India. *Geomorphology* 151–152: 89–98
- Vittori E, Sylos-Labini S, Serva L (1991) Paleoseismology: review of the state of the art. *Tectonophysics* 193:9–32
- Wallace RE (1984) Fault scarps formed during the earthquake of October 2, 1915, in Pleasant Valley, Nevada, and some tectonic implications. *Faulting Related to the 1915 Earthquakes in Pleasant Valley, Nevada, U.S. Geological Survey Prof. Paper, V. 1274-A*, pp 1–33
- Wesnousky SG (1988) Seismological and structural evolution of strike-slip faults. *Nature* 335:340–343
- Wesnousky SG (2000) The role of neotectonics in the study of fault mechanics and seismic hazard. In: *Active fault research for the millenium, Proceedings of the Hokudan International Symposium and School on Active Faulting*, pp 545–552
- Woodcock NH, Fisher M (1986) Strike slip duplexes. *J Struct Geol* 8(7): 725–735
- Whipple KX (2004) Bedrock rivers and the geomorphology of active orogens. *Annu Rev Earth Planet Sci* 32:151–185
- Whipple KX, Di-Biase RA, Crosby BT (2013) Bedrock rivers. *Treatise Geomorphology* 9:550–570
- Wilcox RE, Harding TP, Seely DR (1973) Basic wrench tectonics. *Bull Am Assoc Pet Geol* 57:74–96
- Wilhelmy H (1969) Das Urstromtal am Ostrand der Indusebene und dassarasvati Problem. *Z Geomorphol Supplements* 6 and 8:76–93 (in German)
- Williams RLF (1958) *The Black Hills-Kutch in history and legend*. Weidenfeld and Nicolson, London, pp 276
- Withjack MO, Scheiner C (1982) Fault pattern associated with domes-an experimental and analytical study. *Am Assoc Petroleum Geol* 66(3): 302–316
- Wynne AB (1872) *Memoir on the geology of Kachchh*. Indian Geological Survey Memoir 9:29–47
- Yagi Y, Kikuchi M (2001) Results of rupture process for January 26, 2001, Western India earthquake (Ms 7.9) (Revised). [Http://Www.eic.Eri.U-Tokyo.Ac.jp/Yuji/Southindia/Model1.Html](http://Www.eic.Eri.U-Tokyo.Ac.jp/Yuji/Southindia/Model1.Html)
- Yeats RS, Sieh K, Allen CR (1997) *The geology of earthquakes*. Oxford University Press, New York, 568 pp
- Zheng G, Wang H, Wright TJ, Lou Y, Zhang R, Zhang W, Shi C, Huang J, Wei N (2017) Crustal deformation in the India-Eurasia collision zone from 25 years of GPS measurements. *J Geophys Res Solid Earth* 122(11):9290–9312